

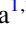


















A Significant Excess in Major Merger Rate for AGNs with the Highest Eddington Ratios at $z < 0.2$

Victor Marian^{1,2} , Knud Jahnke¹ , Irham Andika^{1,2} , Eduardo Bañados¹ , Vardha N. Bennert³ , Seth Cohen⁴ , Bernd Husemann¹ , Melanie Kaasinen^{1,2,5} , Anton M. Koekemoer⁶ , Mira Mechtley⁴ , Masafusa Onoue¹ , Jan-Torge Schindler¹ , Malte Schramm⁷ , Andreas Schulze⁸ , John D. Silverman^{9,10} , Irina Smirnova-Pinchukova^{1,2} , Arjen van der Wel¹¹ , Carolin Villforth¹² , and Rogier A. Windhorst⁴ 

¹Max-Planck-Institut für Astronomie, Königstuhl 17, D-69117 Heidelberg, Germany

²International Max Planck Research School for Astronomy & Cosmic Physics at the University of Heidelberg, Germany

³Department of Physics, California Polytechnic State University, San Luis Obispo, CA 93407, USA

⁴School of Earth and Space Exploration, Arizona State University, P.O. Box 871404, Tempe, AZ 85287-1404, USA

⁵Universität Heidelberg, Zentrum für Astronomie, Institut für Theoretische Astrophysik, Albert-Ueberle-Straße 2, D-69120 Heidelberg, Germany

⁶Space Telescope Science Institute, 3700 San Martin Drive, Baltimore, MD 21218, USA

⁷Graduate school of Science and Engineering, Saitama University, 255 Shimo-Okubo, Sakura-ku, Saitama City, Saitama 338-8570, Japan

⁸National Astronomical Observatory of Japan, Mitaka, Tokyo 181-8588, Japan

⁹Kavli Institute for the Physics and Mathematics of the Universe, The University of Tokyo, Kashiwa, 277-8583 (Kavli IPMU, WPI), Japan

¹⁰Department of Astronomy, School of Science, The University of Tokyo, 7-3-1 Hongo, Bunkyo, Tokyo 113-0033, Japan

¹¹Sterrenkundig Observatorium, Universiteit Gent, Krijgslaan 281 S9, B-9000 Gent, Belgium

¹²University of Bath, Department of Physics, Claverton Down, BA2 7AY, Bath, UK

Abstract

Observational studies are increasingly finding evidence against major mergers being the dominant mechanism responsible for triggering an active galactic nucleus (AGN). After studying the connection between major mergers and AGNs with the highest Eddington ratios at $z = 2$, we here expand our analysis to $z < 0.2$, exploring the same AGN parameter space. Using ESO VLT/FORS2 B -, V -, and color images, we examine the morphologies of 17 galaxies hosting AGNs with Eddington ratios $\lambda_{\text{edd}} > 0.3$, and 25 mass- and redshift-matched control galaxies. To match the appearance of the two samples, we add synthetic point sources to the inactive comparison galaxies. The combined sample of AGN and inactive galaxies was independently ranked by 19 experts with respect to the degree of morphological distortion. We combine the resulting individual rankings into multiple overall rankings, from which we derive the respective major merger fractions of the two samples. With a best estimate of $f_{\text{m,agn}} = 0.41 \pm 0.12$ for the AGN host galaxies and $f_{\text{m,ina}} = 0.08 \pm 0.06$ for the inactive galaxies, our results imply that our AGN host galaxies have a significantly higher merger rate, regardless of the observed wavelength or applied methodology. We conclude that although major mergers are an essential mechanism to trigger local high Eddington ratio AGNs at $z < 0.2$, the origin of $\gtrsim 50\%$ of this specific AGN subpopulation still remains unclear.

Unified Astronomy Thesaurus concepts: [Supermassive black holes \(1663\)](#); [AGN host galaxies \(2017\)](#); [Active galactic nuclei \(16\)](#); [Galaxy mergers \(608\)](#); [Quasars \(1319\)](#); [Galaxy evolution \(594\)](#)

Supporting material: figure set

1. Introduction

An ever-growing number of empirical studies are finding that the properties of the black holes (BHs) at the center of galaxies are closely correlated with the properties of the host galaxy, i.e., BH mass, bulge velocity dispersion and mass, stellar host mass, velocity dispersion, or luminosity (e.g., Marconi & Hunt 2003; Häring & Rix 2004; Jahnke et al. 2009; Bennert et al. 2010, 2011; Beifiori et al. 2012; Graham & Scott 2013; McConnell & Ma 2013; Davis et al. 2018, 2019; de Nicola et al. 2019; Sahu et al. 2019; Ding et al. 2020; Shankar et al. 2020). These findings are complemented by state-of-the-art cosmological hydrodynamical simulations (Habouzit et al. 2019; Terrazas et al. 2020; Li et al. 2020a) that attempt to capture the physics behind these relations. Combined with the widely accepted assumption that every major galaxy hosts a supermassive BH in its center (Kormendy & Ho 2013), this strongly indicates that hierarchical structure formation applies to BHs in the same way as it does to galaxies as a whole (Jahnke & Macciò 2011).

The potential feedback of the emitted radiation, winds, jets, or a combination thereof, when a BH becomes active, (i.e.,

starts accreting matter) may have a broad range of effects on the host galaxy, depending on the physical nature, geometry, and/or size of those different outflow mechanisms (Silk & Rees 1998; Harrison et al. 2018). These range from the total quenching to the enhancement of star formation due to various processes affecting the interstellar and circumgalactic medium (Husemann & Harrison 2018; Weinberger et al. 2018; Nelson et al. 2019; Truong et al. 2020; Davies et al. 2020; Oppenheimer et al. 2020; Valentini et al. 2020), although the impact may also be negligible (Schulze et al. 2019; O’Leary et al. 2020). In addition, individual AGN feedback processes could even have an impact on larger scales by affecting satellite galaxies and the surrounding intracluster or intragroup medium (Blanton et al. 2010; Dashyan et al. 2019; Martin-Navarro et al. 2019; Chowdhury et al. 2020; Li et al. 2020b).

Considering this interplay between galaxies and their central BH in its active phase, it is imperative to understand the mechanisms responsible for triggering the period of significant BH accretion. For decades it has been assumed that galaxies follow an evolutionary path that includes at least one merging event with another galaxy of a similar mass (i.e., a major

merger). This gravitational encounter would strip part of the gas of its angular momentum, funneling it into the most central regions where the BH(s) reside (Barnes & Hernquist 1992; Sanders & Mirabel 1996). Such an incident would ultimately lead to the active galactic nucleus (AGN) phase, in which the coalescing galaxy hosts at least one active BH in the center. This theoretical scenario was comprehensively presented in the seminal work of Sanders et al. (1988), and further studied with numerous simulations (Springel et al. 2005; Hopkins et al. 2006a, 2008; Somerville et al. 2008; McAlpine et al. 2018, 2020; Weigel et al. 2018) and observations (e.g., Yue et al. 2019; Gao et al. 2020). These causal connections, between major mergers and the presence of an active BH, have been found especially for particular AGN populations at low redshift (Koss et al. 2010; Cotini et al. 2013; Sabater et al. 2013; Hong et al. 2015; Ellison et al. 2019), and high-luminosity AGNs at different cosmic epochs (Urrutia et al. 2008; Schawinski et al. 2012; Treister et al. 2012; Glikman et al. 2015; Fan et al. 2016; Donley et al. 2018; Goulding et al. 2018; Urbano-Mayorgas et al. 2019).

In recent years, however, a number of studies have found that the fraction of major mergers among AGN hosts is $< 50\%$, implying that major mergers are not the dominant trigger of AGNs. For example, no predominant connection between major mergers and AGNs could be found for both the general population of X-ray-detected and optically observed AGNs at various redshifts (Gabor et al. 2009; Georgakakis et al. 2009; Cisternas et al. 2011). Likewise, studies that investigated luminosity-selected AGNs with low or moderate X-ray luminosities, with an upper limit of $L_X \leq 10^{43} \text{ erg s}^{-1}$ (Grogin et al. 2005; Allevato et al. 2011; Schawinski et al. 2011; Kocevski et al. 2012; Böhm et al. 2013) or high X-ray luminosities with $L_X \geq 10^{43} \text{ erg s}^{-1}$ (Karouzos et al. 2014; Villforth et al. 2014, 2017) found no significant connection. Studies examining more specific samples of AGNs have obtained similar results: neither sources that possess the highest BH masses (Mechtley et al. 2016) nor heavily obscured AGNs (Schawinski et al. 2012; Zhao et al. 2019) appear to be triggered predominantly by major mergers. Even AGNs assumed to be in an early evolutionary stage (Villforth et al. 2019), or those exhibiting the highest Eddington ratios (Marian et al. 2019) show no signs of an enhanced merger fraction. Additional studies detected slight enhancements in the merger rate for AGNs at different luminosities and redshifts; however, the vast majority of AGNs were still not major merger induced (Silverman et al. 2011; Rosario et al. 2015; Hewlett et al. 2017). In contrast, recent work examining secularly powered outflows (Smethurst et al. 2019) and the dependence of local AGNs on environment (Man et al. 2019) suggest that secular processes are the dominant mechanisms to trigger AGN activity. These studies, in which AGNs with a variety of different redshifts, brightnesses, and masses have been examined, have come to the unanimous conclusion that mergers should only be considered as one of several possible mechanisms for initiating BH growth. Therefore, it is necessary to consider alternative processes and/or differences in the lifetime of merger features and AGNs.

Large-scale galactic bars (Cheung et al. 2015; Cisternas et al. 2015; Goulding et al. 2017) and a time delay between a major merger event and the onset of an AGN (Cisternas et al. 2011; Mechtley et al. 2016; Marian et al. 2019) appear to be an inadequate explanation for these contrary results regarding the

relevance of large-scale mergers for triggering AGNs. Instead, Goulding et al. (2018) propose an intriguing alternative, which may ease this tension: although AGNs are indeed triggered by major mergers, their activity and therefore luminosity during the merging process depend on the merger stage and thus can vary heavily. At larger separations between the two galaxies, the arising torques are not sufficient to provide enough gas to trigger an AGN phase or feed the BH(s). However, at close passages the torques as well as the gas inflow increase, boosting the AGN activity, as long as the distance between the two galaxies is sufficiently small. Before coalescence, this would result in a periodic AGN variability, while the morphological features, like tidal tails, shells, or asymmetries of this encounter would be continuously visible, explaining the lack of observed AGNs in merging systems.

In this study, we investigate the possibility that the AGNs with the highest Eddington ratios $\lambda_{\text{edd}} = L/L_{\text{edd}}$, i.e., the highest specific accretion rates at $z < 0.2$ are predominantly triggered by major mergers. We also expand on the work presented in Marian et al. (2019), in which we studied comparable BHs at $z \sim 2$. Contrary to $z \sim 2$, which marks the peak of cosmic BH activity (Boyle et al. 2000; Aird et al. 2015) and star formation rate (Madau & Dickinson 2014), the comparable population of local AGN host galaxies at $z < 0.2$ exhibit up to ~ 10 times lower BH activity and star formation rates (Aird et al. 2015). Moreover, only a small fraction ($\lesssim 10\%$) of today’s massive galaxies ($\log(M_*/M_\odot) > 10$) may have undergone one or more major merger events since $z \sim 1$, with the majority of such galaxies being undisturbed for the past ~ 7 Gyr (López-Sanjuan et al. 2009; Lotz et al. 2011; Xu et al. 2012). In addition, the mean BH accretion rate (Delvecchio et al. 2015; Aird et al. 2019), as well as the cold gas fraction (e.g., Santini et al. 2014; Popping et al. 2015) of a galaxy are substantially lower at $z < 0.2$ than at $z \sim 2$. Hence, we may expect different physical processes to be dominant at such a low redshift, which makes it necessary to also examine the role of major mergers with respect to triggering AGNs at such a cosmic time. Despite the expected small overall merger rates at low redshifts, especially for the particular population of AGNs showing the highest Eddington ratio, major mergers may still be the only viable option to deliver enough gas to the BH for it to reach such high specific accretion rates.

Like in almost all the aforementioned studies that reject major mergers as the dominant triggering mechanism of AGNs, we compare a specific sample of AGN host galaxies to a sample of inactive comparison galaxies, matched in redshift, stellar mass, observed wavelength, depth, and signal-to-noise ratio (S/N). We examine 17 galaxies hosting AGNs with $\lambda_{\text{edd}} > 0.3$ at $z < 0.2$ and 25 inactive control galaxies and compare the relative difference of the respective merger fractions in order to conclude whether major mergers play a dominant role. We derive the merger fractions by having experts visually classify and rank a joint-blinded and randomized sample with respect to the appearance of distinct (major) merger features, such as tidal tails, shells, or asymmetries, which serve as proxies for an ongoing or recent past merger event. We then create a “consensus ranking” and subsequently split the sample again into AGN hosts and inactive galaxies in order to determine the separate fraction of distorted sources as the basis for discussion.

All magnitudes are given in the AB system and we adopt a concordance cosmology, with $\Omega_\Lambda = 0.7$, $\Omega_0 = 0.3$ and

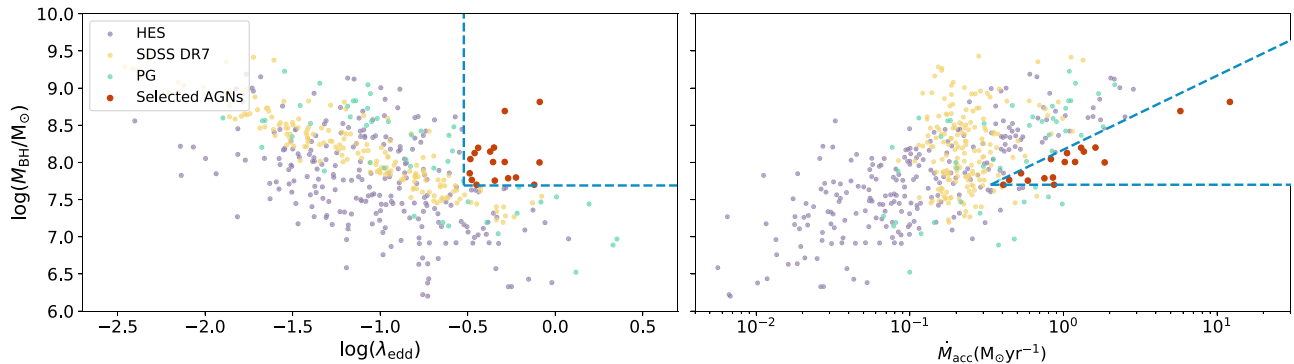


Figure 1. Left: Eddington ratio $\lambda_{\text{edd}} = L/L_{\text{edd}}$ vs. BH mass for the parent sample of AGNs at redshift $z < 0.2$. Overplotted are our selection limits in BH mass and Eddington ratio (blue box) and our final selection of AGNs (red dots). Right: BH mass accretion rate vs. BH mass for the same sample indicating that our final selection consists of AGNs possessing the highest specific accretion rates.

$h = 0.7$. At our sample’s median redshift of $z \sim 0.15$, B - and V - approximately correspond to rest-frame U - and B -band.

2. Data

We base the sizes of our two samples on the goal to identify a potential predominant presence of major merger signatures in AGN host galaxies with respect to a matched sample of inactive galaxies. As a fiducial initial condition, we assume a merger fraction for our control sample of inactive sources of $f_{\text{m,ina}} = 0.15$ with the goal to be able to detect for an AGN host galaxy merger fraction of $f_{\text{m,agn}} \geq 0.5$ a significance difference between these two fractions with $\sim 99\%$ confidence. As the confidence of a detected difference in merger fractions can only increase for smaller values of $f_{\text{m,ina}}$ and to ensure we achieve this desired level of confidence, we use this, when compared to literature results (e.g., Lotz et al. 2011; Man et al. 2016; Mundy et al. 2017), rather large value for $f_{\text{m,ina}}$. We expect this fiducial fraction to be an upper limit of the real merger rate for inactive galaxies in our mass and redshift range.

Since the number of available AGNs with high Eddington ratios at $z < 0.2$ is limited, we first create our sample of AGN host galaxies and then derive the number of inactive galaxies required to satisfy our conditions. With our final sample sizes we can then conclude whether or not AGN host galaxies show a significant enhancement in merger rates, indicating a causal dependence of our population of AGNs on major mergers.

2.1. AGN Host Galaxies

We construct our parent AGN sample by making use of the catalogs provided by the Hamburg/ESO survey (HES, Schulze & Wisotzki 2010), the Palomar Green Survey (PG, Vestergaard & Peterson 2006), and the SDSS DR7 (Shen et al. 2011). We constrain our selection of potential targets to sources with a redshift of $z < 0.2$. Since we require an estimate of the central BH mass and are interested in the AGNs with the highest specific accretion rates, we only select unobscured broadline AGNs with an Eddington ratio $\lambda_{\text{edd}} = L/L_{\text{edd}} > 0.3$. To derive λ_{edd} , we use the BH mass determinations based on single-epoch $H\beta$ measurements and the bolometric luminosities, which, in turn, are based on the luminosities at 5100 \AA multiplied by a bolometric correction factor of $k_{\text{bol}} = 9$ (Schulze & Wisotzki 2010; Netzer 2019). Both the BH masses and luminosities at 5100 \AA are taken from the respective catalogs.

We apply a minimum BH mass threshold of $\log(M_{\text{BH}}/M_{\odot}) = 7.7$, which results in a median BH mass for our AGN sample of $\log(M_{\text{BH}}/M_{\odot}) \sim 8.0$. Using the $M_{\text{BH}} - M_{\text{bulge}}$ scaling relation of Kormendy & Ho (2013) as a proxy to predict stellar host galaxy masses, the corresponding median stellar mass for our AGN host galaxies yields $\log(M_{*}/M_{\odot}) \sim 11$. This mass selection results in feasible exposure times for our inactive galaxies, which are required to be of equal stellar mass, and enables us to compare the results presented in this work with the findings of Marian et al. (2019), which are based on similar stellar host masses. Furthermore, we only select targets with a decl. of $\text{dec} < +15^{\circ}$ for better visibility with the VLT. All of these constraints yield a total number of 19 suitable AGN host galaxies, of which we observe 17 with VLT FORS2 in V - and B -band (ESO programs 091.B-0672(A), 095.B-0773(A), and 098.A-0241(A), PI: Knud Jahnke). The median redshift of these 17 sources lies at $z = 0.15$.

The left panel of Figure 1 summarizes our selection process. The smaller colored points show the respective parent catalogs (with HES in violet, PG in green, and SDSS in yellow) whereas the blue box shows the limits of our parameter space. Our final target selection is indicated by the red points. Since our AGNs show high Eddington ratios ($\lambda_{\text{edd}} > 0.1$), we do not have to consider a potential trend of decreasing radiative efficiency η with low accretion rates (Churazov et al. 2005; Weinberger et al. 2018; Nelson et al. 2019) and can calculate the BH mass accretion rates \dot{M}_{acc} (Figure 1, right panel) as

$$\dot{M}_{\text{acc}} = L/\eta c^2, \quad (1)$$

where we define L as the derived bolometric luminosities and assume an efficiency parameter $\eta = 0.1$. The right panel of Figure 1 highlights that we target the AGNs with the highest specific accretion rates, i.e., those with the highest absolute mass accretion rates relative to their BH masses.

Each target has been observed for at least three long exposures, to detect large-scale distortion features down to B and $V \sim 23.4 \text{ mag arcsec}^{-2}$, and three short exposures, for an unsaturated image of the bright central region. The actual individual exposure times amount to 430 s and 14 s for B and 150 s and 8 s for V , respectively. In Table 1, we summarize the properties of our AGN sample. We cite the corresponding catalog designations, redshifts, apparent I -band magnitudes, as well as the luminosities at 5100 \AA , L_{5100} , and the bolometric luminosities, derived by applying a correction factor of 9 to L_{5100} (Schulze & Wisotzki 2010; Netzer 2019). In addition, we

Table 1
AGN Sample Properties

AGN Designation	z	m_I	L_{5100}	L_{bol}	FWHM	M_{BH}	λ_{edd}	\dot{M}_{acc}
(1)	(2)	mag (3)	erg s ⁻¹ (4)	log(L_{\odot}) (5)	H β (km s ⁻¹) (6)	log(M_{\odot}) (7)	(8)	M_{\odot} yr ⁻¹ (9)
HE0119–2836	0.12	14.8	44.92	12.29	3363.00	8.2	0.36	1.3
HE0132–0441	0.15	15.8	44.81	12.18	1719.00	8.0	0.44	1.0
HE0157+0009	0.16	16.1	44.73	12.10	2369.00	7.8	0.60	0.9
HE0444–3449	0.18	16.0	44.83	12.20	1714.00	8.1	0.35	1.1
HE0558–5026	0.14	15.5	44.88	12.25	1583.40	8.0	0.51	1.2
HE1201–2408	0.14	16.8	44.45	11.82	1820.86	7.8	0.33	0.4
HE1226+0219	0.16	13.2	45.89	13.26	3835.03	8.8	0.82	12.1
HE1228+0131	0.12	14.4	44.93	12.31	1866.19	8.1	0.43	1.4
HE2011–6103	0.12	16.3	44.53	11.90	2862.51	7.9	0.32	0.5
HE2152–0936	0.19	14.2	45.56	12.93	2183.42	8.7	0.52	5.8
HE2258–5524	0.14	15.9	44.68	12.05	2419.42	7.8	0.54	0.8
PG1001+054	0.16	16.3	44.74	12.11	1700.00	7.7	0.76	0.9
PG1012+008	0.19	16.2	45.01	12.38	2615.00	8.2	0.45	1.6
PG1211+143	0.09	14.3	45.07	12.44	1817.00	8.0	0.81	1.9
SDSS-J032213.89+005513.4	0.18	16.1	44.72	12.09	2440.00	8.0	0.33	0.8
SDSS-J105007.75+113228.6	0.13	15.7	44.57	11.94	1906.00	7.8	0.45	0.6
SDSS-J124341.77+091707.1	0.19	16.8	44.41	11.78	1979.00	7.7	0.36	0.4

Note. Properties of the AGNs in our sample: columns 1–3, 6, and 7 are taken from the respective catalogs (Vestergaard & Peterson 2006; Schulze & Wisotzki 2010; Shen et al. 2011). The bolometric luminosities L_{bol} in column 5 are calculated by applying a bolometric correction factor of 9 to L_{5100} (Schulze & Wisotzki 2010; Netzer 2019). Column 6 presents the FWHM of the broad component of H β . We calculate the Eddington ratios λ_{edd} and BH mass accretion rates \dot{M}_{acc} in columns 8 and 9 by using the bolometric luminosities L_{bol} , the respective BH masses M_{BH} , and a radiative efficiency parameter of $\eta = 0.1$.

state the catalog values for the FWHM of the single-epoch measurements of the (broad) H β line, the respective BH masses M_{BH} , along with the calculated Eddington ratios λ_{edd} and mass accretion rates \dot{M}_{acc} .

2.2. Inactive Comparison Sample

Given the size of the AGN sample and our assumptions for the merger fractions for our AGN and control sample ($f_{\text{m,agn}} \geq 0.5$ and $f_{\text{m,ina}} = 0.15$), we need to observe at least 25 inactive galaxies to meet our criterion of detecting a difference in those merger fractions with $\sim 99\%$ confidence. The comparison galaxies are randomly chosen from a parent sample of ~ 2900 galaxies, which are part of the SDSS MPA/JHU catalog (Kauffmann et al. 2003; Brinchmann et al. 2004). We perform this initial selection by constraining the decl. to $\text{dec} < 10^\circ$ and the redshift to $z < 0.2$, resulting in a median redshift of $z \sim 0.13$ for our control sample. Furthermore, we only choose sources that possess comparable stellar masses to our AGN host galaxies. As described in Section 2.1, we adopt the $M_{\text{BH}} - M_{\text{bulge}}$ scaling relation of Kormendy & Ho (2013) to derive the median stellar mass for the AGN sample from the inferred BH masses. We restrict the inactive galaxies to a small range around the median derived stellar mass of the AGN host galaxies, $\log(M_*/M_{\odot}) = 11 \pm 0.01$. Finally, we vet all potential sources against hard X-ray AGN signatures (Baumgartner et al. 2013) to remove any galaxies with a hidden, obscured AGN. In Table 2 we provide the coordinates, redshifts, k -corrected, and dereddened I -band magnitudes, and median stellar masses from the MPA-JHU catalog for our comparison galaxies.

With the exception of one source,¹³ all of the 25 galaxies in our final sample were observed in the B - and V -band with a comparable observational setup as for our AGN host galaxies.

Table 2
Comparison Galaxy Sample Properties

Galaxy Designation	α (J2000)	δ (J2000)	z	m_I	M_*
(1)	deg (2)	deg (3)	(4)	mag (5)	log(M_{\odot}) (6)
Gal000232	0.164	−0.013	0.08	16.9	11.0
Gal003114	2.083	−0.772	0.16	17.8	11.0
Gal030481	19.605	−9.962	0.11	17.8	11.0
Gal050873	34.151	−8.233	0.18	18.1	11.0
Gal079769	50.365	−6.309	0.16	18.0	11.0
Gal095873	58.093	−6.748	0.09	16.6	11.0
Gal176221	132.158	7.598	0.13	17.9	11.0
Gal185580	133.941	3.320	0.12	17.2	11.0
Gal204260	137.351	9.810	0.16	18.0	11.0
Gal210148	138.539	4.123	0.14	17.3	11.0
Gal221730	140.921	−0.891	0.14	18.5	11.0
Gal270096	150.303	−0.089	0.10	17.5	11.0
Gal286443	153.515	7.057	0.10	17.2	11.0
Gal347112	164.300	6.874	0.14	17.7	11.0
Gal391560	171.878	−2.142	0.10	17.1	11.0
Gal419090	176.075	−1.720	0.11	17.1	11.0
Gal458007	181.927	1.421	0.11	17.5	11.0
Gal498251	188.551	−1.446	0.16	17.7	11.0
Gal510223	190.692	0.540	0.08	17.0	11.0
Gal510224	190.692	0.540	0.08	17.0	11.0
Gal534882	195.327	−0.937	0.19	18.2	11.0
Gal557614	199.167	9.361	0.17	17.8	11.0
Gal656010	215.724	8.849	0.14	17.3	11.0
Gal676011	218.892	0.672	0.11	17.2	11.0
Gal698144	222.606	6.647	0.16	18.0	11.0
Gal782980	236.689	−0.860	0.07	16.1	11.0

Note. Our designations (column 1), coordinates (columns 2 and 3), redshifts (column 4) k -corrected and dereddened I -band magnitudes (column 5), and photometric median stellar masses for the inactive galaxies in our comparison sample taken from the MPA-JHU catalog (Kauffmann et al. 2003; Brinchmann et al. 2004).

¹³ Due to weather losses one target was only observed in V -band.

Each target has been observed with at least three individual, 470 s and 180 s long, exposures in B and V , respectively. This selection and observational approach enables us to analyze two distinct samples of AGN host galaxies and inactive comparison galaxies, which are nonetheless matched in redshift, stellar (host) mass, depth, spatial resolution, filter band, and S/N. Thus, we can directly compare potential relative differences in the merger fractions of both populations.

2.3. Data Reduction and Preparation

We require a seeing of $1''$ or better to diagnose large-scale merger signatures at a minimum required spatial resolution of ~ 2.5 kpc at our sample’s median redshift. Hence, prior to reducing the raw images, we automatically determine the average seeing for each exposure by measuring the FWHM of 100 local peaks, using the `Astropy` package `photutils` (Bradley et al. 2019), and calculating the corresponding median FWHM of all sources. We visually check and remeasure every single exposure with a median FWHM $> 1''$ and discard individual exposures with a median FWHM above this threshold. Out of a total of ~ 450 individual frames, we reject 22 from the subsequent reduction process and analysis. Despite the exclusion of these images, we end up with at least three individual exposures per band for every object.

To execute all the initial data reduction steps, i.e., the bias and flat-field correction, sky background subtractions, astrometry, and aligning, and combination of individual exposures, we use the data processing pipeline THELI¹⁴ (Erben et al. 2005; Schirmer 2013). The resulting pixel scale of $0''.252$ corresponds to ~ 0.6 kpc at our median redshift. We combine the respective B - and V -band observations to create color images using `MultiColorFits`¹⁵ (Cigan 2019).

To ensure that the samples are directly comparable, we mimic the appearance of the AGN host galaxies in the images of the inactive galaxies by adding a synthetic point source on top of the respective flux centers. To this end, we first detect the 15 brightest, unsaturated stars within the central image regions around each inactive galaxy with the help of the `DAOSStar-Finder` algorithm within the `photutils` package. For each galaxy, we then visually select and cut out one of the detected stars, and upscale the brightness correspondingly, such that they possess a central brightness comparable to HE2152–0936, our second brightest AGN source. In the course of this procedure we also downscale noise in the outer parts. Since an upscaling with a constant factor would lead to a noticeable discrepancy in flux between the galaxy and the edge of the artificially enhanced point source, we fit the original point sources with a two-dimensional Gaussian and determine a circular region centered around the brightest pixel with a radius of 5σ . We divide this region into five bins and upscale the pixel values depending upon which bin they lie in. For the innermost region, i.e., within 1σ , we upscale with the total scaling factor, whereas for the outermost region, i.e., between 4 and 5σ we apply a scaling factor lower by 5×10^{-4} . For the intermediate bins we choose a multiple of the scaling factor such that the distribution of the scaling factor with radius follows a Gaussian function. Using this approach, we create point sources that resemble the central regions of our AGN host galaxies, but also

blend in unrecognizably and smoothly into the respective galaxies. We add these point sources randomly at the centroid of each inactive galaxy, mimicking the appearance of our AGN host galaxies. Our point sources have a similar size to the upper limit of $\sim 1''$ set on the seeing, whereas the typical diameter of our sample galaxies, both AGN and inactive, is of the order of 5 – $6''$. Thus, in contrast to our study of highly accreting AGNs at $z \sim 2$ (Marian et al. 2019) there was no necessity to model and subtract point sources for the samples here.

Examples of an AGN host galaxy and an inactive comparison galaxy are shown in Figure 2. The left (a) and middle column (b) depict the V - and B -band images, respectively, whereas the right column (c) shows the color images. To optimize the visibility of large-scale structures and possible merger signatures, while blending out the brightest inner regions, we chose different parameters for the color cuts and color map for the single band images as well as the color images. However, within one set, i.e., V -, B -band or color images, the parameters are constant. In addition, we adopted a Gaussian two-pixel smoothing for the color images only. Due to the different visualization of the sources, we can test for any systematic differences in the subsequent distortion rankings or the resulting merger fractions (see Section 4).

3. Morphological Analysis and Merger Fractions

We join both processed samples (for which the galaxies can no longer be visually separated as AGN or not) resulting in a final sample of 42 sources in V - and 41 in B -band and color, respectively. To derive the merger fractions, 19 experts,¹⁶ proficient in working with imaging data of galaxies, perform a visual assessment of the targets, ranking them from most to least distorted with respect to the appearance of large-scale distortion features. These features are indicative of ongoing or recent major merger events. Each set of V -, B -band, and color images is ranked independently by each expert. We note that there are an increasing number of machine-learning algorithms that can classify galaxies, based on their morphologies and possibly merger state (e.g., Bottrell et al. 2019; Snyder et al. 2019; Cheng et al. 2020). However, we rely on the human interpretation and judgment due to the manageable sample size and the extensive time and logistic requirement to teach an automatic classification routine with a matching “external” training set. Since the sources in the joint sample are indistinguishable with respect to whether or not they are active, every expert’s individual bias regarding the classification of a major/minor merger applies equally to AGN host galaxies and comparison galaxies. Thus, in our subsequent analysis any personal subjectivity in classification will have the same impact on either of the two subsamples. To further reduce any systematic bias, the data set provided to each of the 19 ranking experts is randomized. As an additional task, we request every classifier to choose a “cutoff” rank below which they deem all sources to be in a merging state, or, to at least show signs of a recent gravitational disturbance, like asymmetries, tidal tails, or double nuclei. Every galaxy with a rank higher than the cutoff is interpreted to be completely free of major disturbances stemming from interactions. In our ensuing analysis we will use this property to determine the

¹⁴ <https://www.astro.uni-bonn.de/theli/gui/index.html> <https://github.com/schirmerschicha/THELI>

¹⁵ <https://multicolorfits.readthedocs.io>

¹⁶ The rankings were done by the co-authors Andika, Bañados, Bennert, Cohen, Husemann, Jahnke, Kaasinen, Koekemoer, Marian, Onoue, Schindler, Schramm, Schulze, Silverman, Smirnova-Pinchukova, van der Wel, Villforth, and Windhorst.

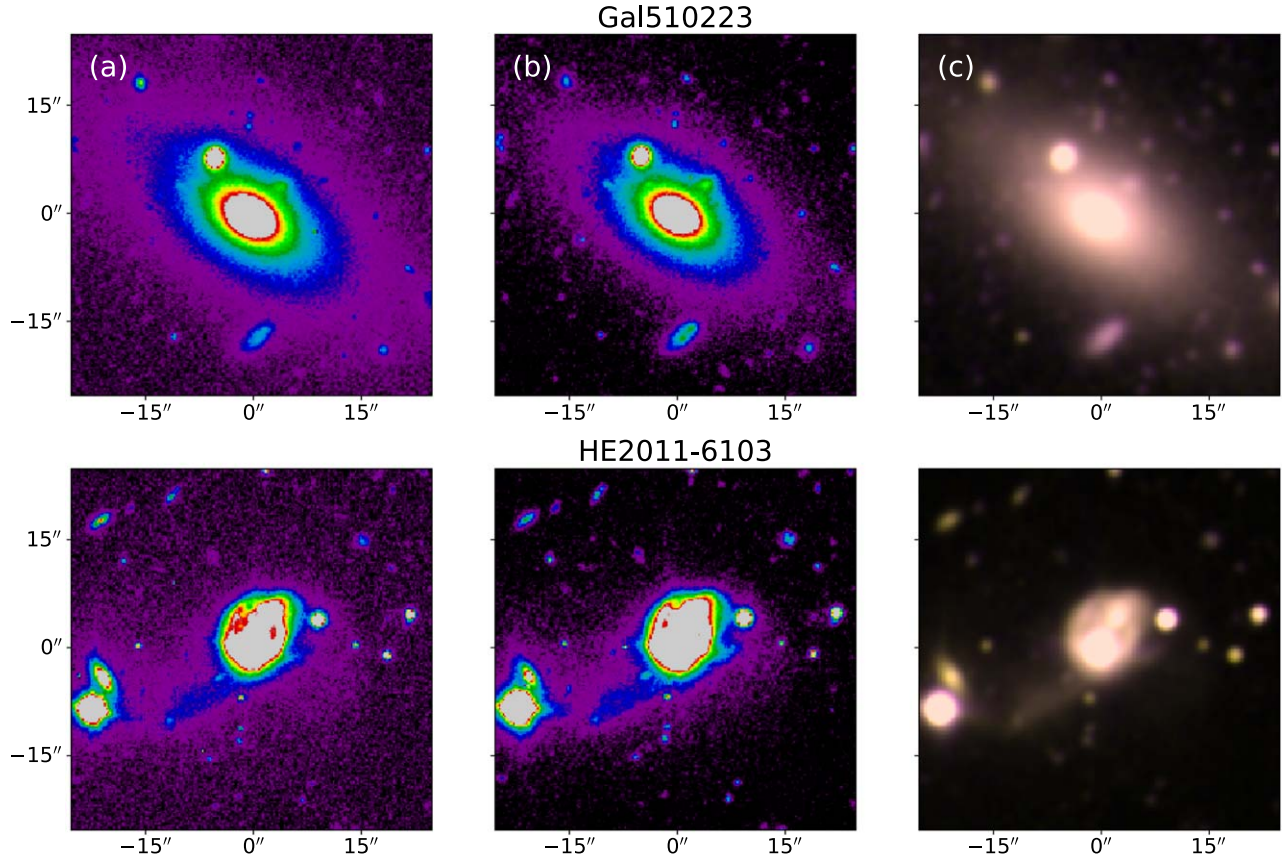


Figure 2. Two sources representative of our targets. On the top row we show one of the comparison galaxies and on the lower row one of our AGNs is displayed. From left to right we present a postage stamp in (a) V -band, (b) B -band, and (c) color, respectively. Note: In order to enhance the visibility the images are not shown with the same cuts and color map parameters.

merger fractions of our two samples and also discuss the dependence of those fractions on different cutoff ranks (see Section 4).

We combine the 57 individual rankings (19 experts times three sets) into three consensus sequences for each respective set. We apply the same methods as in Marian et al. (2019) to combine the individual rankings and repeat this task for each set, i.e., separately for B -, V -band, and color images. For our first approach we calculate and weigh the average ranks of each galaxy, whereas for our second and third approach we use the Borda count (Emerson 2013) and the Schulze algorithm (Schulze 2011, 2018), respectively. More information on the different methods and on how we implement them are provided in Appendix A. Ultimately, by applying all three methods to all three sets we obtain nine overall rankings.

We select various cutoff ranks and split the combined rankings back into AGN host and comparison galaxies. Subsequently, we derive the merger fractions for each chosen cutoff rank by counting how many active and inactive galaxies are above and below this threshold. The merger fraction is then simply defined as,

$$f_m = \frac{a}{a + b}, \quad (2)$$

where a represents the number of merging galaxies, whereas b counts the sources that are undisturbed. However, since we only examine samples of limited size, we need to quantify the probability densities and uncertainties introduced by the shot noise for our resulting merger fractions. Based on those two

parameters, a and b , we can quantify the probability densities for a continuous range of merger fractions in the feasible interval $[0, 1]$ by using the beta distribution (see also Mechtley et al. 2016; Marian et al. 2019),

$$f(x) = \frac{(a + b + 1)!}{a! b!} x^{a-1} (1 - x)^{b-1}. \quad (3)$$

The respective standard deviations and means of the associated merger fraction probability distributions are then derived by,

$$\sigma(x) = \sqrt{\frac{ab}{(a + b)^2(a + b + 1)}}, \quad (4)$$

and Equation (2), respectively.

In Figure 3, we present the corresponding means and standard deviations of the various probability distributions for every combination of method and set for four distinct cutoff ranks at 5, 10, 15, and 20. The merger fractions increase with cutoff rank, because a higher cutoff rank means that more galaxies are below this limit and are thereby considered to exhibit merger features. We find no evidence that the choice of combination method or the choice of B -, V -, or color image set affect the resulting merger fractions. For all combinations the results for a given sample and cutoff rank are well within the errors of each other or even equal. However, it is also evident that for cutoff ranks $\lesssim 15$ the merger fractions for the AGN host galaxies (Figure 3, upper row) are significantly larger than the fraction of disturbed inactive galaxies (Figure 3, bottom row).

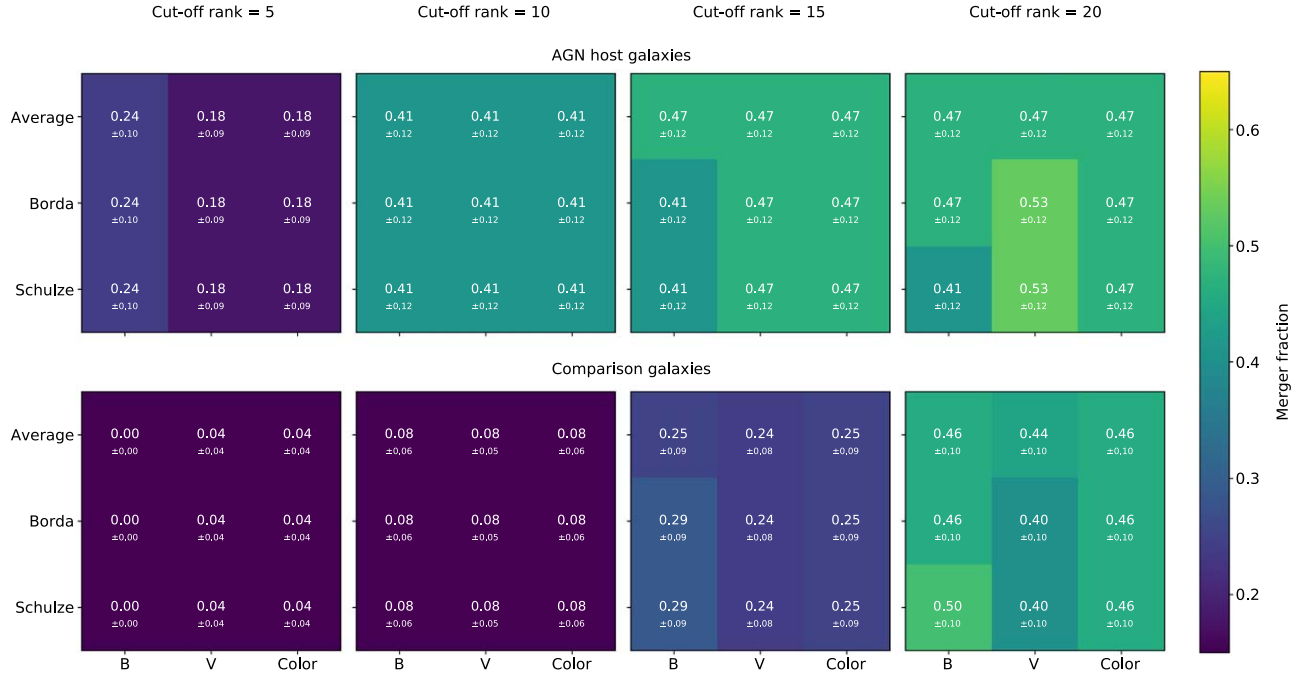


Figure 3. The merger fractions for every set (B –, V –band, and color images) and ranking combination method (average, Borda, Schulze) for four distinct cutoff ranks. In the top row we show the corresponding fractions of disturbed AGN host galaxies, the bottom row depicts analogously the inactive comparison galaxies. The smaller numbers below the actual merger fraction values give the standard deviations (i.e., 1σ) of the corresponding beta distributions.

This is not the case for larger cutoff ranks. We discuss the implications of the chosen cutoff ranks on our recovered merger fractions and the potential causal connection between major mergers and the triggering of AGNs in the following section.

3.1. Constraining the Absolute Merger Fractions

We have calculated the merger fractions for two samples of 17 AGN host galaxies and 25 inactive comparison galaxies. As mentioned in the preceding section, the final merger fractions depend on the choice of cutoff rank. In Appendix B we present the continuous evolution of merger fractions with cutoff rank for all combinations of set and method, while in this section we describe the two approaches we used to analyze and interpret our results. First, we base the cutoff rank on our experts’ opinions, and second, we construct this limit so that the resulting merger fraction of our inactive control sample is consistent with the merger rates presented in the literature. To obtain a valid first estimate, we calculated the means of the individual cutoff ranks chosen by each classifying expert for each set. The average cutoff ranks are 21 ± 8 , 22 ± 9 , and 18 ± 8 for the B , V , and color sets, respectively.

We suspect that the reason for such high cutoff ranks, which are almost bisecting our joint samples, lies in the visual determinations of our experts. Since our galaxies are well resolved, any minor asymmetries (which do not need to stem from a recent major merger event, but can be of a minor merger or secular origin) can be easily identified. This leads our experts to put those particular sources into the “merger bin”, i.e., below the cutoff rank, increasing the percentage of galaxies classified as merging. With a corresponding cutoff rank = 20, the merger fractions range between $f_{m,agn} = 0.41 \pm 0.12$ and $f_{m,agn} = 0.53 \pm 0.12$ for the AGN sample and $f_{m,ina} = 0.40 \pm 0.10$ and $f_{m,ina} = 0.50 \pm 0.10$ for the inactive sample. Therefore, the fractions of disturbed sources in both samples

are not significantly different, which would indicate a negligible contribution of mergers of any strength to the triggering of AGNs.

However, our primary goal is to determine the distinct impact of *major* mergers on the formation of AGNs, without considering the effects of minor gravitational encounters or other processes shaping the morphology of a galaxy. Thus, we have to correct our recovered merger fractions for the contamination by sources with minor asymmetries. Such a high merger rate of $\sim 40\%$ – 50% indicates that approximately half of the population shows signs of a recent or ongoing gravitational encounter of any strength. This significantly exceeds our initial assumption for inactive galaxies (see Section 2) and also the assessments by previous studies (Lotz et al. 2008b, 2008a, 2011; Bridge et al. 2010; Xu et al. 2012; Casteels et al. 2014; Man et al. 2016; Ventou et al. 2017, 2019; Duncan et al. 2019; O’Leary et al. 2020). Based on these studies, we adopt a major merger rate per galaxy of $R_m \sim 0.05$ [Galaxy $^{-1}$ Gyr $^{-1}$]. This number represents the number of galaxies currently in a merger state, divided by the timescale of the visibility of merger signatures. In order to obtain an absolute merger fraction, representative of our comparison sample, we need to multiply this rate with the timescale T_m in which a major merger is observable. This property not only depends strongly on the mass ratio, individual masses, and gas fractions of the two progenitor galaxies, but also on the depth of the observations. Considering our targets’ low redshifts and surface brightness limits, we choose a comparatively conservative value of $t_m \sim 1.5$ Gyr, which results in a major merger fraction of $f_m \sim 0.08$ for galaxies in our mass bin and at our sample’s redshift.

Such a value for the merger fraction for our comparison galaxies corresponds to a cutoff rank = 10. Coincidentally, at this cutoff rank the respective merger fractions are equal over all sets and methods for each of the two samples (Figure 3) and

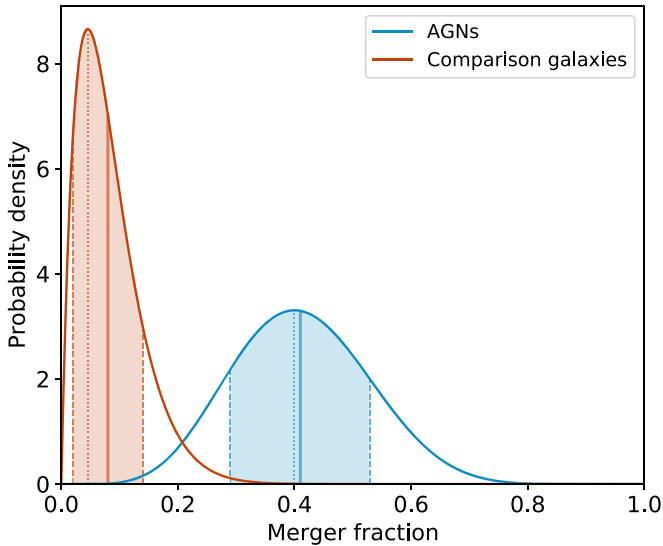


Figure 4. Probability distributions for the derived merger fractions of our $z < 0.2$, high-accretion AGN host galaxies (blue) and inactive galaxies (red) at a cutoff rank = 10. The solid and dotted lines show the means and modes of the respective merger fractions, while the dashed lines and shaded regions depict the central 68% confidence intervals. At this particular cutoff rank the respective merger fractions are identical, independent of method and set.

yield $f_{m,agn} = 0.41 \pm 0.12$ for the AGN host galaxies and $f_{m,ina} = 0.08 \pm 0.06$ for the comparison galaxies. This value of $f_{m,ina}$ is not only in excellent agreement with the major merger rates found in the 3DHST survey by Man et al. (2016) for all five fields (AEGIS, COSMOS, GOODS-N, GOODS-S, UDS) in CANDELS (Grogin et al. 2011; Koekemoer et al. 2011), but also for the major merger fractions recovered by MUSE deep observations (Ventou et al. 2017, 2019) as well as studies by Duncan et al. (2019) in CANDELS, and in GAMA by Mundy et al. (2017).

The two corresponding probability distributions are shown in Figure 4, with blue and red denoting the probability distributions for the AGN sample and the comparison sample, respectively. The shaded regions represent the 1σ intervals and the solid and dotted lines depict the corresponding means and the modes. Due to the low number of merging comparison galaxies, the associated probability distribution appears considerably skewed with the corresponding mean not coinciding with the peak position. Thus, we also report the merger fraction associated with the mode of the distribution, which yields $f_{m,ina} \sim 0.04$ and is still well within the error of the mean.

4. Discussion

4.1. Robustness of Results

For a cutoff at rank 10, the resulting merger fractions translate to,

1. 7/17 AGN host galaxies showing merger features, and
2. 2/25 inactive galaxies showing merger features.

The order and appearance of the sources in the various consensus rankings do not have to be congruent, e.g., the 7 as merger classified AGN host galaxies could vary in the different consensus rankings. However, we find that, despite a difference in order, the first eight positions of every combined ranking feature the same targets, with seven of them being the same AGN host galaxies. Out of these seven targets, five stem from

the HES sample, while one each is listed initially in the SDSS and PG catalogs, respectively. Since we selected a total of 11 AGNs from the HES catalog and in each case three from the SDSS and PG catalogs, we conclude that the parent catalogs from which the AGN host galaxies are drawn from are not introducing any bias with respect to morphological classification. A repeated visual inspection also confirms that a distinction at exactly this cutoff rank into merging and non-disturbed systems reveals a noticeable separation into sources with clearly obvious large-scale merger features like tidal tails and shells and galaxies with explicitly fewer asymmetries.

Eventually, we created one singular overall ranking by re-applying the Schulze method on the nine consensus rankings (see Appendices C and D). The same sources that occupy the first eight ranks in the nine initial consensus sequences, populate the highest positions in this final ranking as well. Therefore, we obtain an unchanged result for both merger fractions after again applying a cutoff at rank 10.

Considering the appearance of seven AGN host galaxies among the eight highest-ranked sources and the clear excess in merger fractions for the AGN host galaxies with respect to the inactive sample with a significant difference of $>2.5\sigma$, we conclude that major mergers are an essential triggering mechanism for AGNs with the highest Eddington ratios at $z < 0.2$. However, based on the mean of our recovered probability distribution for the AGN merger fraction, we only find a $\sim 22\%$ probability that the merger fraction is above the threshold of $f_{m,agn} = 0.5$. This means that although major mergers are indeed a non-negligible mechanism in triggering our specific population of AGNs, more than half of the BHs must be activated by different means, like secular processes or minor mergers. We discuss the role of the latter in triggering AGNs with the highest specific accretion rates at low redshifts in more detail in Section 4.5.

4.2. Comparison to Previous Studies

Our result, which shows an excess in AGN merger fraction compared to a matched control sample, stands in contrast to recent simulations (Steinborn et al. 2018; Ricarte et al. 2019) and several previous empirical studies examining the potential causal connection between major mergers and the triggering of different populations of AGNs. Villforth et al. (2014) found no increase in merger signatures with luminosity and also reported consistent disturbance fractions between the AGNs and comparison galaxies for their sample of observed low- and moderate-luminosity AGNs ($41 \lesssim L_X [\text{erg s}^{-1}] \lesssim 44.5$) at $0.5 \lesssim z \lesssim 0.8$. In contrast, Silverman et al. (2011) found an enhanced merger rate for AGNs of moderate X-ray luminosities in spectroscopic pairs at $z < 1$. However, their rate of $17.8^{+8.4}_{-7.4}\%$ is still significantly lower than what we find here.

AGNs and host galaxies at comparable redshifts and luminosities as our sample were explored by Böhm et al. (2013) and Grogin et al. (2005). They assessed the neighboring counts, asymmetries, and various morphological indices (concentration, Gini coefficient, and M_{20} index) to characterize the respective host galaxies, but found no significant causality between major mergers and AGNs. Likewise, Allevalo et al. (2011), Schawinski et al. (2011), and Rosario et al. (2015) detected no redshift evolution of morphological properties for similar AGNs up to $z \sim 2.5$ and Kocevski et al. (2012) found that only $16.7^{+5.3}_{-3.5}\%$ of comparable AGNs at $z \sim 2$ are highly disturbed. X-ray-selected and optically observed AGNs with

higher luminosities ($43 \lesssim L_X [\text{erg s}^{-1}] \lesssim 46$) at $0.5 \lesssim z \lesssim 2.2$ also appear to show no causal link to major mergers (Cisternas et al. 2011; Hewlett et al. 2017; Villforth et al. 2017). Instead, they all reported consistent merger fractions of $\sim 15\%$ – 20% . Regarding more specific populations at $z \sim 2$, Schawinski et al. (2012) presented a major merger fraction between 4% and 11% for their analyzed sample of 28 dust-obscured AGNs, while Mechtley et al. (2016) has found consistent merger fractions for 19 galaxies hosting the most massive supermassive BH ($M_{\text{BH}} = 10^9 - 10^{10} M_{\odot}$) and a sample of 84 matched inactive galaxies. Similarly, in our previous work (Marian et al. 2019) in which we examined 21 AGNs with the highest Eddington ratios ($\lambda_{\text{edd}} > 0.7$) at $z \sim 2$ and compared them to 92 matched inactive galaxies, we found no dominant connection between major mergers and the occurrence of AGNs.

Similar to the results presented in this work, other studies have found considerably enhanced merger rates for particular populations of AGNs. For their sample of hard X-ray detected, moderate luminous AGNs at $z < 0.05$ Koss et al. (2010) reported an enhanced merger fraction of 18% when compared to a matched control sample, in which only 1% of the sources display merger features. However, they speculated that their AGNs may not be classified correctly via means of optical diagnostics due to superimposing features of ongoing star formation and optical extinction. In fact, it appears that independent of redshift, obscured, and luminous AGNs are more likely to be connected to major merger events. Albeit, it should be noted that this is expected because by focusing on obscured sources a bias toward merging systems is most likely introduced as that obscuration may be due to dust within a merging (U)LIRG-like host. With this caveat in mind, Glikman et al. (2015), Fan et al. (2016), and Donley et al. (2018) detected merger fractions $> 50\%$ for such reddened or obscured AGNs sources at $z \sim 2$, $z \sim 3$, and $0 < z < 5$, respectively. Also, at low redshifts ($z \lesssim 0.2$), Koss et al. (2018) and Ellison et al. (2019) presented comparable results. In addition, in the latter study the authors described an increase of merger fraction with AGN luminosity, with the most luminous AGNs exhibiting the highest merger incidence. Corresponding findings have also been reported by Treister et al. (2012), Hong et al. (2015), and Goulding et al. (2018), who have analyzed luminous AGNs ($\log(L_{\text{bol}} [\text{erg s}^{-1}]) > 45$) at various redshifts. Especially with a merger fraction of $\sim 44\%$ for luminous AGNs at $z < 0.3$, the results published in Hong et al. (2015) are very consistent with the distortion rate we find for our sample of AGNs of comparable bolometric luminosity. Similar results are also reported by Gao et al. (2020) for their sample of AGNs at $0 < z < 0.6$, who detected a merger fraction of $\sim 40\%$ and a general increase of distortion incidence with stellar mass. Finally, McAlpine et al. (2018, 2020) reported for the EAGLE simulation that major mergers—while of no great importance at high redshifts—play a significant role at low redshifts and present a consistent major merger fraction of $\sim 40\%$ for BHs growing rapidly at $z \sim 0$.

4.3. Physical Interpretation and Comparison to AGN Counterparts at $z \sim 2$

In light of our previous work at $z \sim 2$ (Marian et al. 2019), which also focuses especially on AGNs with the highest Eddington ratios, but yields an opposite result, we need to consider the different epochs of the studied AGNs. To make a

comparison in absolute terms between the AGN major merger fractions, which we recover for the respective two samples at $z \sim 2$ and $z < 0.2$, we have to factor in the impact of surface brightness dimming on detecting possible faint morphological distortion features. With a drop in surface brightness of $\sim 5 \text{ mag arcsec}^{-2}$ at $z \sim 2$, at this redshift we most definitely miss merger features we otherwise would see at $z \sim 0.2$. This effect can be enhanced by the fact that galaxies at $z \sim 2$ are on average more compact than at $z \sim 0$ (e.g., van der Wel et al. 2014). If the triggering of an AGN follows immediately after a starburst caused by a galaxy merger, the resulting potential extensive amount of dust can obscure the starburst at $z \sim 2$ more easily than at $z \sim 0.2$. In the latter case, the starburst may happen as much in the galaxy’s outer spiral arms and tidal streams, whereas the starburst in a galaxy at $z \sim 2$ is much more confined to the central region due to its more compact nature. Hence, in addition to the difference in surface brightness dimming between $z \sim 2$ and $z \sim 0.2$, a more complex situation is possible where the visibility of an AGN host galaxy at $z \sim 2$ is not only reduced by surface brightness dimming, but also by obscuring dust. Thus, the AGN merger fraction at $z \sim 2$ could be significantly underestimated with $f_{\text{m,agn}} = 0.24 \pm 0.09$ for the AGN sample at $z \sim 2$ and $f_{\text{m,agn}} = 0.41 \pm 0.12$ for the AGNs presented in this study (see Section 3.1). Therefore, this effect could explain the discrepancy in the derived AGN major merger rates and would lead us to the conclusion that a substantial part of AGNs with the highest Eddington ratios at $z \sim 2$ is actually triggered by major mergers as well. However, in Marian et al. (2019) as well as in this study we draw our main conclusions by comparing the respective AGN samples to two matched control samples of inactive galaxies at both redshifts and determining primarily the relative differences between the respective merger fractions. The corresponding merger fractions for the inactive galaxies are $f_{\text{m,ina}} = 0.19 \pm 0.04$ and $f_{\text{m,ina}} = 0.08 \pm 0.06$ for the sources at $z \sim 2$ and $z \sim 0.2$ (see Section 3.1), respectively.

We assume now that the actual merging process is independent of the presence of a potential future AGN and consider the mechanisms causing the detectable morphological features to be identical between the respective AGN host galaxies and their corresponding inactive counterparts. As a result, the merger fractions at $z \sim 2$ are affected equally by surface brightness dimming and we actually do not have to consider this effect. Similarly, a merger-driven starburst creating an abundant amount of obscuring dust can happen equally in both an inactive galaxy or a system that will host an AGN triggered by this merger event. Hence, dust would only impact the findings described in Marian et al. (2019) if the dust were to obscure the actual AGNs, which would lead to a misclassification of those particular sources as inactive galaxies. In this earlier study, however, we investigated the importance of hidden and intermittent AGNs at $z \sim 2$, which would implicitly include such sources, but found no significant effect on the resulting merger rates. In addition, just as in this work, we deliberately have only selected type-1 AGNs, minimizing the probability of dust-obscured sources influencing the reported result. We expect the number of such sources with a dust content low enough to be not classified as type-2 AGNs, but sufficiently high to actually hide a potential AGN or morphological merger features to be relatively low. Therefore, similar to the surface brightness dimming, we can neglect the effect of obscuring dust when considering the relative

difference in merger fractions at $z \sim 2$. A rigorous analysis would require a larger sample and data at longer wavelengths, as the James Webb Space Telescope (JWST) will be able to provide at $z \sim 2$, enabling spatial modeling of dust in more detail.

Since we only compare the relative differences in merger fractions at both redshifts with no significant distinction of merger fractions at $z \sim 2$, but a clear excess of the AGN merger fraction when compared to inactive galaxies at $z < 0.2$, we still conclude that major mergers play an essential role for AGNs with high Eddington ratios at low redshift. In addition, the major merger fractions for both samples of inactive galaxies are consistent with previous findings of major merger rates for galaxies at comparable redshifts and masses by Man et al. (2016), Snyder et al. (2019), Steinborn et al. (2018), and Ventou et al. (2017, 2019). This agreement corroborates the findings presented in Marian et al. (2019) and indicates that surface brightness dimming or dust is actually not impacting the merger fractions at $z \sim 2$ considerably. Hence, we have to consider an alternative explanation for this excess of merger fraction in our subpopulation of AGNs at low redshift.

Besides the mean BH accretion rate/bolometric luminosity and Eddington ratio of an AGN (Schulze et al. 2015), especially the cold gas fraction of a galaxy at $z < 0.2$ is considerably lower than for a counterpart at $z \sim 2$ (e.g., Santini et al. 2014; Popping et al. 2015). Hence, with the AGNs in both redshift samples having comparable Eddington ratios, but the sources at lower redshifts a significant smaller intrinsic gas reservoir it is reasonable to assume that while at $z \sim 2$ a sufficient amount of gas is still left to fuel the central supermassive BH via other mechanisms than major mergers, at $z < 0.2$ this process is essential to trigger AGNs with the highest specific accretion rates. This scenario is completely consistent with the results of the EAGLE simulations, which see major mergers in a negligible role for triggering AGNs at high redshifts, but shows that such galaxy encounters play a substantial role at low redshifts, yielding comparable major merger fractions (McAlpine et al. 2018, 2020). However, it should be noted that despite the excess in major merger fraction for our AGN host galaxies, $\gtrsim 50\%$ of our sample appear not to be not triggered by such an event, requiring an alternative explanation for the existence of such AGNs.

4.4. AGN Merger Fraction and Luminosity

Although our AGN sources can be considered luminous for sources at $z < 0.2$, we emphasize that we have not selected our AGNs on absolute luminosity (see Section 2.1 for our sample selection). Rather, we have chosen the AGNs with the highest Eddington ratios, i.e., the sources with the highest accretion rates and luminosities relative to their BH masses. Except for the two AGNs—HE1226+0219 and HE2152–0936, which possess bolometric luminosities of $\log(L_{\text{bol}}[\text{erg s}^{-1}]) > 46.5$ —all our remaining sample AGNs have luminosities of $45.3 \lesssim \log(L_{\text{bol}}[\text{erg s}^{-1}]) \lesssim 46$, but feature the smallest BH masses in that luminosity bin ($7.7 < \log(M_{\text{BH}}/M_{\odot}) < 8.2$). In fact, ~ 10 more luminous AGNs in our three initial parent catalogs would have been selectable. Unlike other studies, which detect an enhanced merger rate for luminous AGNs we see no trend of the strength of the merger features—i.e., rank—with either BH mass or BH mass accretion rate/luminosity within our AGN sample (Figure 5). In fact HE1226+0219 and HE2152–0936, both with distinctly higher absolute mass

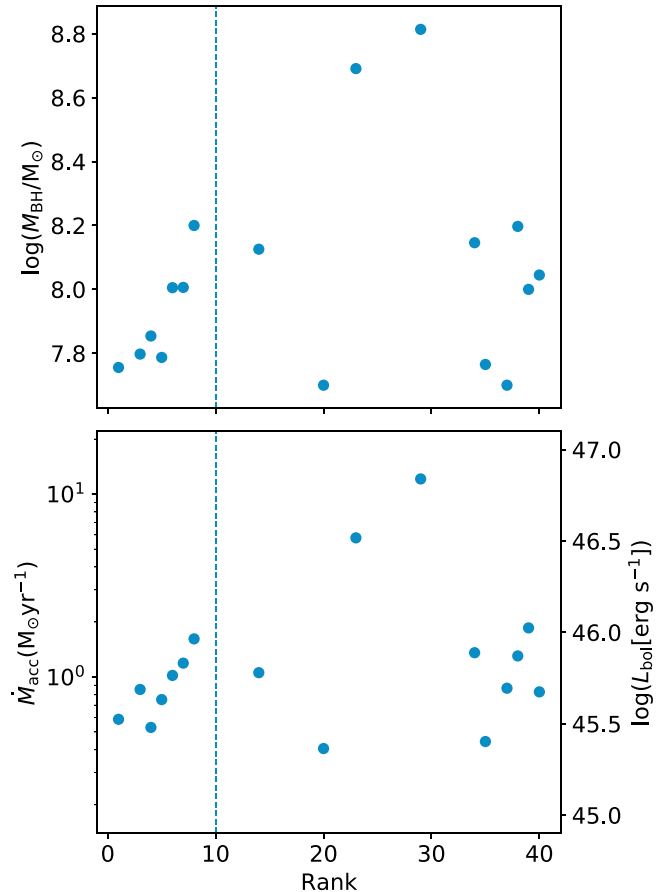


Figure 5. Overall consensus rank vs. BH mass (top) and BH mass accretion rate and bolometric luminosity (bottom) for our sample of AGNs. The vertical dashed line visualizes a cutoff at rank 10, which was used in our discussion.

accretion rates with respect to our other sample AGNs, only occupy the ranks ~ 30 and ~ 25 in all the consensus rankings and show clearly no significant merger features. However, due to our selection of AGNs being based on a combination of BH mass and Eddington ratio, we note that apart from the two aforementioned most luminous AGNs our sources sample a relatively narrow luminosity range. Still, because of the lack of an obvious correlation of merger fraction with AGN luminosity, our results require an alternative explanation—especially considering that the existence of such a trend is still inconclusive. Despite some studies finding evidence of such a link between merger rate and luminosity (Treister et al. 2012; Fan et al. 2016; Goulding et al. 2018), others did not (Villforth et al. 2014, 2017; Hewlett et al. 2017).

4.5. The (Un)Importance of Minor Mergers

In Section 3.1 we argue that the initial high merger fraction of our sample of control galaxies is the result of our experts including galaxies in the merger category, which show features that are only the consequence of minor merger events. Lotz et al. (2011) state that the minor merger rate is \sim three times the major merger rate (with a minor merger being in a mass ratio range of $1:4 < M_{\text{sat}}/M_{\text{primary}} \lesssim 1:10$). Considering our major merger fraction for those galaxies to be correct we end up with a *total* merger fraction of $f_{\text{m,ina}} = 0.33 \pm 0.09$ for our inactive galaxies. This would correspond to a cutoff at a rank of 17 and in turn in a total merger fraction of $f_{\text{m,agn}} = 0.47 \pm 0.12$ for our

AGN host galaxies. Obviously the difference between these two distortion rates is significantly decreased and indeed for our singular overall ranking we find eight inactive galaxies and eight AGNs below our cut at rank 17. However, while all experts can easily agree on the most distorted galaxies, it should be noted that sources with such small asymmetries are more difficult to classify. Hence, the rank of a particular galaxy with such features may differ strongly in the individual expert's rankings, which in turn could also influence to some extent the resulting overall rank and hence also the actual number of sources being considered merging in our final ranking. Nevertheless, we do not expect this scatter to be substantial. With only one AGN host galaxy, but eight inactive galaxies added into the merger category, it appears that only a small fraction of AGNs are seen to be in this interval. Hence, we are confident that the number of AGN host galaxies showing weak distortion features is still significantly less than compared to our comparison galaxies. This points to the conclusion that minor merging is comparably unimportant and most of the rest of AGNs require a different triggering mechanism.

4.6. Considering AGN and Merger Timescales

With major mergers only triggering at most $\sim 50\%$ of our AGNs and minor mergers playing a subdominant role, the question still remains which process(es) are responsible for triggering high Eddington rate AGNs at $z < 0.2$. With that question in mind and a diminishing number of alternative mechanisms we consider a possible impact of the different timescales. Previous studies, which have found no enhancement in distortion fractions between AGNs and a matched sample of control galaxies, analyzed a potential disparity in AGN and merger lifetimes to be an explanation for their results (Cisternas et al. 2011; Mechtley et al. 2016; Marian et al. 2019). The unanimous conclusion is that the difference in life cycles is not sufficient to explain the lack of excess in merger rates, since the timescale of merger features being observable is much longer than the lifetime of the respective AGNs.

We consider a scenario in which some of the galaxies that host no visible AGN and feature only minor distortions are actually the result of a major merger event which also lead to a past phase of active BH growth. However, since the lifetime of AGNs can be significantly shorter when compared to that of major merger features, the only detectable remains of such a gravitational encounter would be in the form of minor asymmetries. This implies that if we utilize the *total* merger fractions we derived in the previous subsection, a part of the $33 \pm 9\%$ inactive galaxies that show distortions of various strength have actually hosted a major merger triggered AGN in the past. As a result, the AGN major merger fraction with $f_{m,agn} = 0.41 \pm 0.12$ would increase, indicating that major mergers are not only an essential, but indeed the dominant mechanism to trigger high Eddington rate AGNs at $z < 0.2$.

Following the scenario outlined by Goulding et al. (2018), we also assess the number of AGNs in an ongoing merger after first passage that are currently not visible due to an insufficient gas inflow. Those particular BHs will eventually become active again when the distance between the two galaxies decreases again resulting in growing torques and hence gas inflow. As in Marian et al. (2019), we refer to such AGNs in the following as intermittent AGNs. We cannot distinguish between such AGNs or past AGNs that will not be ignited again. However, since we

are only interested in the eventual increase of the AGN merger fraction, the origin of this increase is irrelevant.

We try to constrain the fraction of distorted inactive galaxies, which hosted an AGN in the recent past or currently an intermittent AGN, $f_{m,ina\&agn}$ by adopting the formula presented in Marian et al. (2019):

$$f_{m,ina\&agn} = f_{agn} \times f_{m,agn} \times \frac{t_m}{t_{agn}}. \quad (5)$$

Here, f_{agn} and t_{agn} represent the fraction and lifetime of AGNs with an Eddington ratio $> 30\%$ with respect to the total galaxy population at our redshift and mass bin. The timescale in which the merger features are observable is given by t_m , while $f_{m,agn}$ describes the total merger fraction of our specific AGN population. We derive f_{agn} by utilizing the number densities provided by stellar mass and quasar bolometric luminosity functions at $z \sim 0$ and our stellar mass range and average bolometric AGN luminosity. Using the respective median *I*-band magnitudes this yields $\log \Phi \sim -2.9 \text{ Mpc}^{-3} \text{ mag}^{-1}$ for the total galaxy population (Hirschmann et al. 2014; Furlong et al. 2015; Henriques et al. 2015; Lacey et al. 2016; Pillepich et al. 2018) and $\log \Phi \sim -5.8 \text{ Mpc}^{-3} \text{ mag}^{-1}$ for our particular population of AGNs (Hopkins et al. 2007; Fanidakis et al. 2012; Hirschmann et al. 2014; Sijacki et al. 2015), resulting in $f_{agn} \sim 1.3 \times 10^{-3}$, which is in excellent agreement with the value for the active fraction reported by Schulze & Wisotzki (2010) for BHs at a redshift $z < 0.3$ and a mass of $\log(M_{BH}/M_{\odot}) \sim 8$. For $f_{m,agn}$ we use our reported value of $f_{m,agn} = 0.47 \pm 0.12$, but also repeat our calculations for $f_{m,agn} = 0.30$ and 0.70 . Besides our initial estimate of $t_m = 1.5 \times 10^9 \text{ yr}$ (see Section 3.1), in addition, we use $t_m = 10^9 \text{ yr}$ for comparison. Finally, in accordance to previous studies we constrain our AGN lifetime t_{agn} to a range between 10^6 and 10^8 yr (Martini 2004; Hopkins et al. 2005; Shen et al. 2007; Hopkins & Hernquist 2009; Conroy & White 2013; Cen & Safarzadeh 2015). Since we cannot distinguish between inactive merging galaxies that already went through their AGN phase, are yet to host an AGN, or are currently hosting an intermittent AGN, it is not necessary for us to consider any time lag (Hopkins et al. 2006b; Wild et al. 2010; McAlpine et al. 2020) between the onset of the actual phase of active BH growth and the beginning/coalescence of the merger. Hence, from the perspective of timescales our result solely depends on the relative difference between the AGN and merger lifetimes and thus we have to consider our fraction of inactive merging galaxies, which have hosted an AGN to be an upper limit. However, a visual re-examination returned only a low number of galaxies with asymmetries actually having a close companion. Therefore, we conclude that most of the distorted galaxies are already in the late stages of their merging process, indicating that, if at all, they already experienced a potential AGN phase with a low chance of an intermittent AGN becoming active again.

The total merger fraction of our inactive galaxies, which amounts to $f_{m,ina} \sim 0.35$, serves as an upper bound for $f_{m,ina\&agn}$. Both parameters being equal would imply that all distorted, inactive galaxies have hosted (or will host) an AGN. Conversely, $f_{m,ina\&agn} = 0$ would correspond to no such galaxy ever hosting an AGN. In Figure 6 we present the results of our computations for different $f_{m,agn}$ and $t_m = 10^9 \text{ yr}$ (left) and $1.5 \times 10^9 \text{ yr}$ (right). The blue lines and the shaded regions denote the results for our retrieved AGN merger

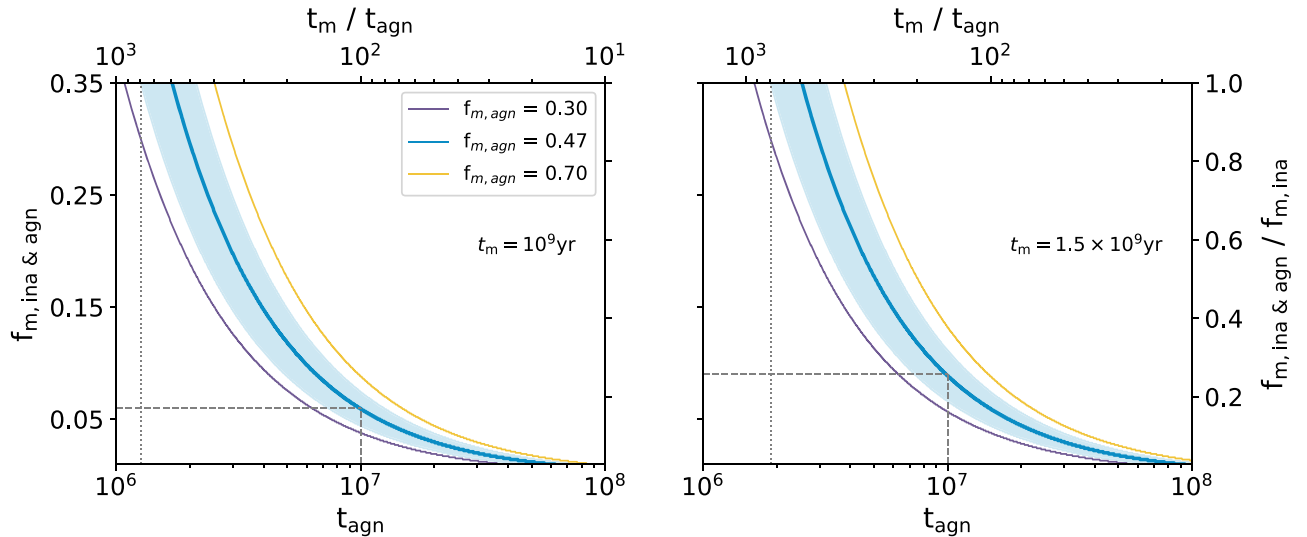


Figure 6. Total fraction of merging inactive galaxies that hosted an AGN in the recent past $f_{m,ina&agn}$ in dependence of the AGN lifetime t_{agn} for a merger timescale t_m of 10^9 yr (left) and $t_m = 1.5 \times 10^9$ yr (right). The blue line including the shaded region represents our result of the AGN total merger fraction of $f_{m,agn} = 0.47 \pm 0.12$. The violet and yellow lines correspond to $f_{m,agn} = 0.30$ and 0.70 , respectively. The dotted line corresponds to a lower limit of t_{agn} , the dashed lines display the resulting $f_{m,ina&agn} \sim 0.09$ for an assumed $t_{agn} = 10^7$.

fraction and the corresponding 1σ intervals, while the violet and yellow lines display the trend for $f_{m,agn} = 0.30$ and 0.70 , respectively. The fraction of merging inactive galaxies hosting an AGN at some point during the merging process increases with shorter AGN lifetimes. In addition, for a given period of AGN activity this share grows with longer merger timescales and larger AGN merger fractions, both due to an enhanced probability to find a distorted galaxy actually hosting an AGN. Depending on the merger timescale and assuming the lower limit of our AGN merger fraction is correct, we can deduce a lower bound for the AGN lifetime by considering every inactive distorted galaxy to host an AGN, i.e., $f_{m,ina&agn} \equiv f_{m,ina}$. The life span of an AGN corresponds then to a minimum of 1.3×10^6 yr and 1.9×10^6 yr for merger timescales of 10^9 yr and 1.5×10^9 yr, respectively (Figure 6, dotted lines).

However, based on the best estimates for accretion rate histories we have today (Di Matteo et al. 2005; Johansson et al. 2009a, 2009b; Hopkins & Quataert 2010; Jung et al. 2018), we fix the time period in which an AGN accretes above $\lambda_{edd} > 0.3$ to $t_{agn} = 10^7$ yr. The inferred fractions of inactive merging galaxies that also host an AGN at any given time yield then $f_{m,ina&agn} = 0.06_{-0.02}^{+0.01}$ and $0.09_{-0.02}^{+0.02}$ for $t_m = 10^9$ yr and 1.5×10^9 yr, respectively (Figure 6, dashed lines). So, adding even the upper limit of this fraction onto the AGN major merger rate we derived in Section 3.1 this only results in a revised AGN major merger fraction, which is barely above the threshold of 0.5, which in turn would indicate that the majority of AGNs are triggered by major mergers. This result still leaves $\sim 50\%$ of AGNs to be of unknown origin. Only by assuming a significantly lower AGN duty cycle of $t_{agn} \sim 10^6$ yr and thus regarding almost every distorted inactive galaxy hosting an AGN, we can obtain AGN major merger fractions of $\sim 80\%$, which would then leave no doubt about the role of major mergers and the triggering of high Eddington rate AGNs at $z < 0.2$. Hence, we conclude that neither a difference in AGN and merger timescales nor the potential presence of intermittent AGNs affect significantly our derived AGN merger rate. In order to better constrain our inferred estimates, more detailed

simulations predicting especially AGN timescales in dependence of accretion rate are imperative.

5. Summary and Conclusions

We examined a potential direct connection between AGNs specifically exhibiting the highest Eddington ratios and major mergers at $z < 0.2$. We analyzed 17 AGN host galaxies and 25 comparison galaxies, matched in mass, redshift, filter, and the S/N in V , B , and color images. We adjusted our control galaxies by adding artificial point sources on top of their flux centers, which yielded two indistinguishable samples, that were joined to create a randomized overall sample of 42 targets. This overall sample was ranked according to the presence of merger features (from most to least distorted) by 19 experts. We combined the individual rankings of each set, i.e., V , B and color, by applying three different methods, resulting in a total number of nine consensus rankings. This allowed us to determine any bias, which might be introduced by visually classifying the galaxies at different wavelengths or the algorithm to combine the individual classifications. Finally, we also created one overall sequence by combining the nine initial consensus rankings. We divided all rankings into: (1) galaxies showing distinct merger features and (2) galaxies showing no signs of a gravitational disturbance, by choosing specific cutoff ranks. As a final step, we derived the respective merger fractions by counting the numbers of active and control galaxies above and below these particular limits and applying those quantities to a beta distribution.

Our findings depend heavily on the choice of distinction between merging and undisturbed systems. To analyze how the selection of the cutoff rank affected our result, we: (1) selected it based on the visual interpretations by the experts and (2) chose it such that the merger rate of our comparison sample was consistent with the overall major merger fraction of galaxies in our mass and redshift range. When we considered the average determinations of the classifiers, approximately half of both populations showed signs of a current or recent merger event, suggesting no causal connection between major

mergers and the triggering of this particular population of AGNs.

Since our first approach also considers asymmetries or signatures that stem from processes other than a major merger event, we adjust the major merger fraction of the inactive galaxies to be consistent with recent simulations and observations. As a result, we find a substantial excess in the major merger fraction of the AGN sample with respect to the inactive galaxies. Coincidentally, with a separation at the corresponding cutoff rank, we also found a clear distinction between strongly disturbed galaxies and galaxies with either minor or no merger signatures, confirming our classification.

We summarize our findings as follows.

1. The merger fractions of the AGN host galaxies and comparison galaxies are $f_{m,agn} = 0.41 \pm 0.12$ and $f_{m,ina} = 0.08 \pm 0.06$, respectively.
2. Neither the choice of set nor combination method has impacts the recovered merger fractions.
3. For our AGNs, with the highest Eddington ratios at $z < 0.2$, major mergers are an essential mechanism to trigger BH growth.
4. We rule out that minor mergers play a considerable role in the triggering of our subpopulation of AGNs.
5. Considering AGN and merger lifetimes as well as AGN variability induced by an ongoing merger event, our best estimate results in $\sim 50\%$ of our AGN population still being of unknown origin.

Extending our study to include integral field unit (IFU) observations and a larger number of sources would enable us to analyze the AGN host galaxies in more detail. By assessing the strength of potential past merger events by examining the kinematics and stellar populations, while larger number provides better statistics we can determine, which processes are responsible for the triggering of the remaining $\sim 50\%$ and whether major mergers are indeed the dominant mechanism.

We thank the referee for the constructive feedback, which improved the quality of this work.

We also thank Mischa Schirmer for his helpful guidance in using THELI.

J.S. is supported by JSPS KAKENHI grant No. JP18H01251 and the World Premier International Research Center Initiative (WPI), MEXT, Japan. V.N.B. gratefully acknowledges assistance from a National Science Foundation (NSF) Research at Undergraduate Institutions (RUI) grant (AST-1909297). Note that findings and conclusions do not necessarily represent views of the NSF. R.A.W. acknowledges support from NASA JWST Interdisciplinary Scientist grants NAG5-12460, NNX14AN10G and 80NSSC18K0200 from GSFC.

Based on observations made with ESO Telescopes at the La Silla Paranal Observatory under program ID 091.B-0672, 095. B-0773 & 098.A-0241.

Funding for the Sloan Digital Sky Survey (SDSS) has been provided by the Alfred P. Sloan Foundation, the Participating Institutions, the National Aeronautics and Space Administration, the National Science Foundation, the U.S. Department of Energy, the Japanese Monbukagakusho, and the Max Planck Society. The SDSS Web site is <http://www.sdss.org/>.

The SDSS is managed by the Astrophysical Research Consortium (ARC) for the Participating Institutions. The

Participating Institutions are The University of Chicago, Fermilab, the Institute for Advanced Study, the Japan Participation Group, The Johns Hopkins University, Los Alamos National Laboratory, the Max Planck Institute for Astronomy (MPIA), the Max Planck Institute for Astrophysics (MPA), New Mexico State University, University of Pittsburgh, Princeton University, the United States Naval Observatory, and the University of Washington.

This research has made use of NASA’s Astrophysics Data System Bibliographic Services.

Facility: ESO-VLT(FORS2).

Software: astropy (Astropy Collaboration et al. 2013, 2018), Matplotlib (Hunter 2007), MultiColorFits (Cigan 2019), SAOI-mageDS9 (Joye & Mandel 2003), THELI (Erben et al. 2005; Schirmer 2013).

Appendix A Details on Combination Methods

Every method to combine individual votes into a combined consensus sequence violates at least one of three criteria described by Arrow’s impossibility theorem (Arrow 1950). It states that no existing method, which combines two or more individual votes satisfies the following three axioms: (1) non-dictatorship, such that all individual votes are considered to be equal; (2) unanimity or the weak Pareto principle, stating that if all voters agree on $X > Y$, this also holds true for the overall ranking; and (3) the independence of irrelevant alternatives, such that the consensus relation between X and Y only depends on the individual preferences between those two entities and not any additional option(s). As additional conditions we introduce the Condorcet paradox and the Condorcet criterion (Condorcet 1785; Condorcet et al. 1989). The first one states that an overall sequence can be cyclic—e.g., X wins over Y , which wins over Z , which in turn wins over X —although the individual votes are not. The latter explains that an overall top-ranked candidate wins in every pairwise comparison with every other candidate.

Below we present the methods we apply to create the overall rankings. As stated in Section 3, we use three different algorithms to construct those combined rankings to determine any potential bias introduced by the method. However, in addition all of our three methods also satisfy or infringe the above mentioned criteria differently, which gives us even more detailed insights in any potential introduction of differences in the merger fractions.

For our first method to combine the individual expert rankings we adopt the same method applied in Mechtley et al. (2016) and Marian et al. (2019). We start with calculating the mean rank for each galaxy from the individual rankings and discard every individual expert classification of each galaxy, if it differs more than 2σ from the respective average rank. Out of the 798 individual assessments in V -band we reject 25 votes, while out of the total 779 ratings, 17 are discarded for the sets in B -band and color, respectively. However, since we weigh individual votes this method obviously violates the non-dictatorship criterion.

Our second method, the Borda count approach (Emerson 2013), satisfies this condition, but violates in exchange the independence of irrelevant alternatives. We adapt the original version of this method in which the first-ranked option receives n points, the second one $n - 1$ and so on, with n being the total

number of candidates, by applying the Dowdall system (Reilly 2002). With that approach the candidates receive the reciprocal value of their respective ranks, i.e., the first-ranked option is rewarded $1/n = 1$ point, the next one 0.5 points, and so on. As low-rank galaxies may be ranked more randomly due to a lack of significant merger features, we can decrease the impact those sources might have on our overall ranking by using this variant of the Borda count.

This approach avoids the Condorcet paradox, but only our third method, the Schulze method (Schulze 2011, 2018), also satisfies the Condorcet criterion. With this method all pairwise comparisons between two candidates X and Y for all individual rankings are calculated and put into relation to each other, resulting in an overall ranking, where the top-ranked candidate, wins indeed over all other candidates, being the so-called Condorcet winner. Going to lower ranks within the resulting consensus sequence the second-placed candidate only loses to the first-ranked option and so on (for more details and examples please see Schulze 2018).

Appendix B Dependence of Merger Fractions on Cutoff Rank

In Sections 3 and 4 we describe how the choice of cutoff rank can influence the resulting merger fractions and also present for four selected cutoff ranks the corresponding merger fractions. In Figure 7 we now present the continuous dependence of merger fractions on cutoff rank for all combinations of method and set. The AGN host galaxies and inactive galaxies are shown in blue and red, respectively. The shaded regions denote the 1σ confidence interval from shot and classification noise. As already indicated in Figure 3 and described in Section 3, it is also shown in Figure 7 that first, neither the choice of method to combine the individual rankings nor the selection of set has any significant impact on the resulting absolute merger fractions or the relative differences between them. Second, compared to the inactive comparison sample and for cutoff ranks $\lesssim 15$, the AGN host galaxies show a clear excess in merger fractions. This clearly indicates that our conclusions rely considerably on the choice of cutoff rank, which is extensively discussed in the main text.

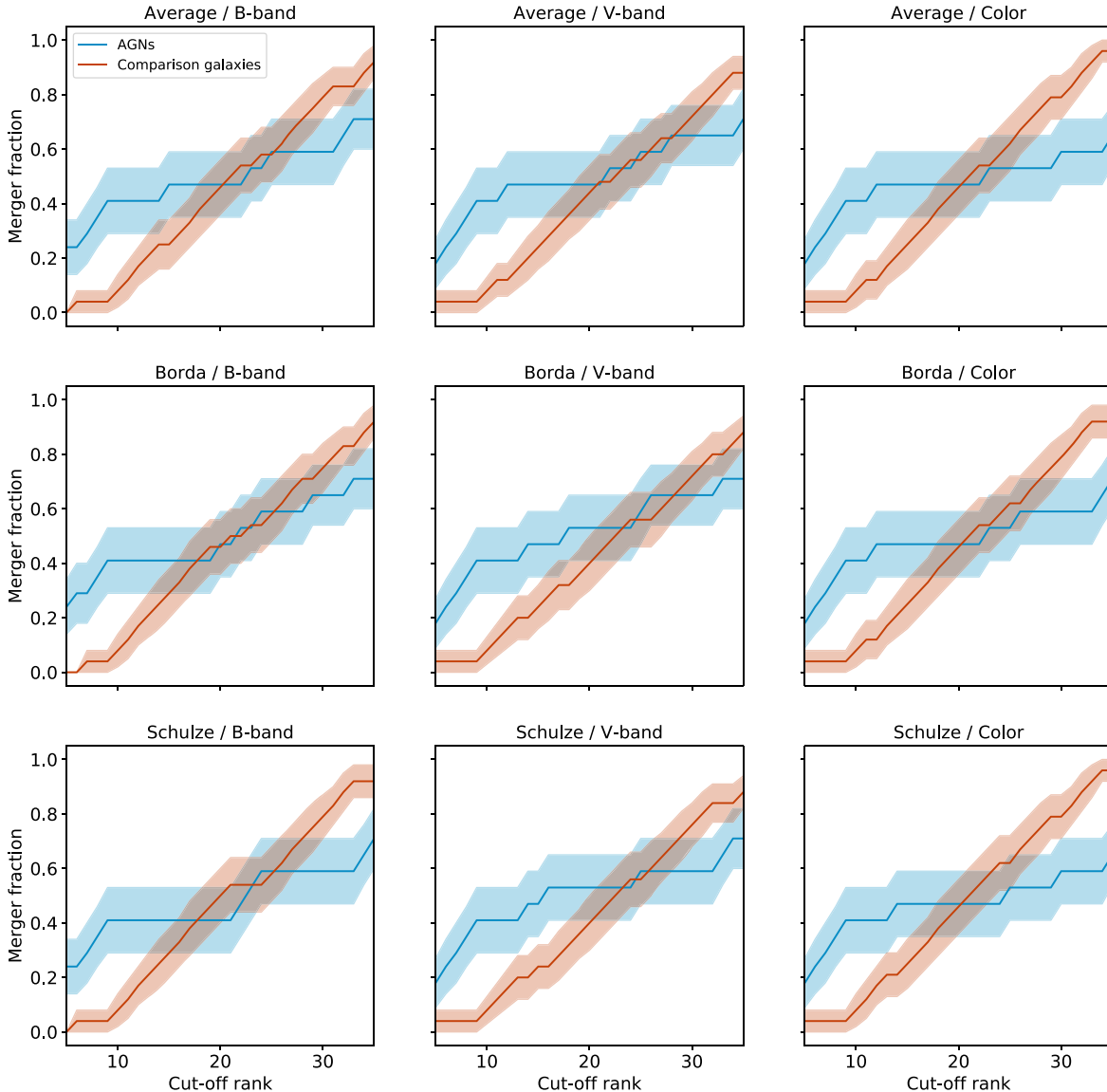


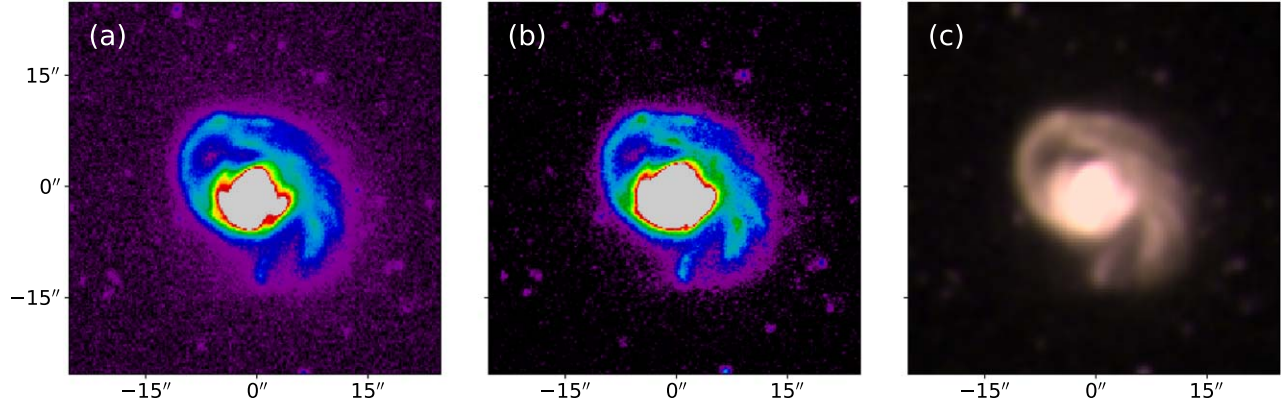
Figure 7. Evolution of the merger fractions for the AGN host galaxies (blue) and inactive galaxies (red) in dependence of cutoff rank for each combination of set and method. The shaded regions give the 1σ confidence interval.

Appendix C Visual Overall Consensus Ranking

To have a “meta” singular consensus sequence we apply the Schulze method (see Section 3 and Appendix A) to our final nine overall rankings, which we calculated for each combination of set and method. We show all sources in the resulting order (Figure 8; complete figure set available online), and include for completeness also the sources

already shown in Figure 2. The respective rank for each object is given in parentheses besides its designation. It should be noted that Gal176221 is only ranked last, because it was only observed in *V*-band and therefore only appears in the three corresponding consensus rankings. In those three respective rankings it is always positioned at rank 14. Clearly visible is the drop off in strong merger features at a cutoff rank $\gtrsim 10$.

(1) - SDSSJ105007.75+113228.6



(2) - Gal030481

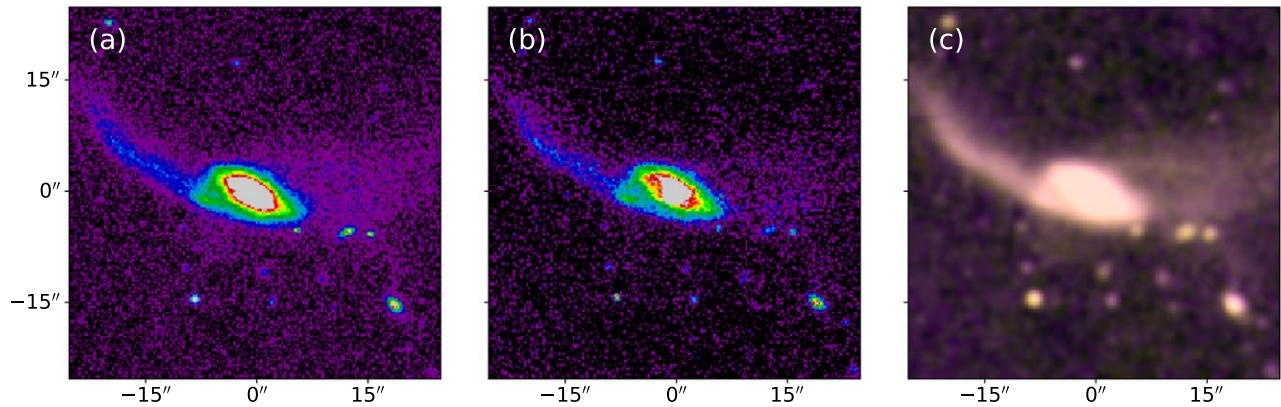


Figure 8. From left to right we present a postage stamp in (a) *V*-band, (b) *B*-band, and (c) color, respectively. Note: In order to enhance the visibility the images are not shown with the same cuts and color map parameters. The complete figure set (42 images) is available in the online journal.

(The complete figure set (42 images) is available.)

Appendix D
Tabular Overall Consensus Rankings

Complementary to Appendix C we present in this section for referential use the consensus ranks for each target for all sets

and combination methods (Table 3). As in Appendix C the sources are sorted by rank of the “meta” consensus ranking, i.e., the combined ranking of the nine overall rankings (see Section 4.1).

Table 3
Final Consensus Ranks

Target	Borda			Average			Schulze		
	V-band	B-band	Color	V-band	B-band	Color	V-band	B-band	Color
SDSS-J105007.75+113228.6	1	3	3	1	4	4	1	3	5
Gal030481	4	6	1	2	5	1	2	5	1
HE0157+0009	3	1	4	3	1	6	3	1	6
HE2011-6103	2	2	5	4	2	5	4	2	4
HE2258-5524	5	4	2	6	6	2	5	4	2
HE0132-0441	7	7	6	5	7	3	6	7	3
HE0558-5026	6	5	8	7	3	8	7	6	8
PG1012+008	8	8	7	8	8	7	8	8	7
Gal458007	10	11	9	9	10	9	9	10	10
Gal079769	12	10	10	13	9	13	10	9	9
Gal270096	11	12	12	10	11	12	11	11	11
Gal698144	18	13	13	15	12	10	18	12	12
Gal782980	9	9	15	12	13	16	12	13	16
HE0444-3449	13	21	11	11	22	11	13	21	13
Gal534882	15	16	16	20	19	18	17	17	15
Gal510223	19	14	21	17	15	19	22	14	19
Gal050873	20	17	17	19	20	17	19	18	17
Gal419090	22	22	18	18	18	15	20	16	18
Gal676011	23	15	20	23	16	21	23	15	20
SDSS-J124341.77+091707.1	17	19	22	21	14	22	15	22	24
Gal498251	21	18	26	22	17	25	21	19	22
Gal286443	16	20	27	16	21	26	16	20	23
HE2152-0936	24	23	37	24	24	35	24	23	35
Gal185580	26	30	14	25	29	14	25	28	14
Gal003114	28	24	29	28	23	27	27	24	26
Gal204260	31	26	19	29	26	20	30	29	21
Gal347112	30	29	23	26	27	23	26	26	27
Gal557614	27	27	24	30	28	24	28	27	25
HE1226+0219	25	28	25	27	31	29	33	33	29
Gal095873	29	31	32	31	30	31	29	30	32
Gal210148	33	25	35	33	25	33	31	25	33
Gal221730	34	33	28	32	33	28	35	32	31
Gal000232	36	34	30	37	34	32	34	31	30
HE1228+0131	35	32	33	34	32	37	36	34	36
HE1201-2408	37	38	34	35	36	34	32	36	34
Gal391560	38	39	31	36	39	30	38	35	28
PG1001+054	32	36	41	38	35	40	37	37	39
HE0119-2836	40	37	39	39	37	38	39	38	38
PG1211+143	39	35	38	40	38	39	40	39	41
SDSS-J032213.89+005513.4	41	40	40	41	40	41	42	40	40
Gal656010	42	41	36	42	41	36	41	41	37
Gal176221	14	N/A	N/A	14	N/A	N/A	14	N/A	N/A

Note. The final ranks for each source depending on combination method (Borda, average, or Schulze) and set (*B*, *V* or color images). The targets are sorted by a repeated use of the Schulze method on this nine overall rankings resulting in a singular consensus sequence. Since we have for Gal176221 only observations in *V*-band it is ranked last by the algorithm.

ORCID iDs

Victor Marian  <https://orcid.org/0000-0003-1733-9281>
Knud Jahnke  <https://orcid.org/0000-0003-3804-2137>
Irham Andika  <https://orcid.org/0000-0001-6102-9526>
Eduardo Bañados  <https://orcid.org/0000-0002-2931-7824>
Vardha N. Bennert  <https://orcid.org/0000-0003-2064-0518>
Seth Cohen  <https://orcid.org/0000-0003-3329-1337>
Bernd Husemann  <https://orcid.org/0000-0003-2901-6842>
Melanie Kaasinen  <https://orcid.org/0000-0002-1173-2579>
Anton M. Koekemoer  <https://orcid.org/0000-0002-6610-2048>
Mira Mechtley  <https://orcid.org/0000-0001-6462-6190>
Masafusa Onoue  <https://orcid.org/0000-0003-2984-6803>
Jan-Torge Schindler  <https://orcid.org/0000-0002-4544-8242>
Malte Schramm  <https://orcid.org/0000-0001-7825-0075>
Andreas Schulze  <https://orcid.org/0000-0002-6660-6131>
John D. Silverman  <https://orcid.org/0000-0002-0000-6977>
Irina Smirnova-Pinchukova  <https://orcid.org/0000-0002-2260-3043>
Arjen van der Wel  <https://orcid.org/0000-0002-5027-0135>
Carolyn Villforth  <https://orcid.org/0000-0002-8956-6654>
Rogier A. Windhorst  <https://orcid.org/0000-0001-8156-6281>

References

- Aird, J., Coil, A. L., Georgakakis, A., et al. 2015, *MNRAS*, 451, 1892
Aird, J., Coil, A. L., & Georgakakis, A. 2019, *MNRAS*, 484, 4360
Allevato, V., Finoguenov, A., Cappelluti, N., et al. 2011, *ApJ*, 736, 99
Arrow, K. J. 1950, *Journal of Political Economy*, 58, 328
Astropy Collaboration, Price-Whelan, A. M., Sipőcz, B. M., et al. 2018, *AJ*, 156, 123
Astropy Collaboration, Robitaille, T. P., Tollerud, E. J., et al. 2013, *A&A*, 558, A33
Barnes, J. E., & Hernquist, L. 1992, *ARA&A*, 30, 705
Baumgartner, W. H., Tueller, J., Markwardt, C. B., et al. 2013, *ApJS*, 207, 19
Beifiori, A., Courteau, S., Corsini, E. M., & Zhu, Y. 2012, *MNRAS*, 419, 2497
Bennert, V. N., Auger, M. W., Treu, T., Woo, J.-H., & Malkan, M. A. 2011, *ApJ*, 742, 107
Bennert, V. N., Treu, T., Woo, J.-H., et al. 2010, *ApJ*, 708, 1507
Blanton, E. L., Clarke, T. E., Sarazin, C. L., Randall, S. W., & McNamara, B. R. 2010, *PNAS*, 107, 7174
Böhm, A., Wisotzki, L., Bell, E. F., et al. 2013, *A&A*, 549, A46
Bottrell, C., Hani, M. H., Teimoorinia, H., et al. 2019, *MNRAS*, 490, 5390
Boyle, B. J., Shanks, T., Croom, S. M., et al. 2000, *MNRAS*, 317, 1014
Bradley, L., Sipocz, B., Robitaille, T., et al. 2019, *astropy/photutils: v0.7.2*, Zenodo, doi:10.5281/zenodo.3568287
Bridge, C. R., Carlberg, R. G., & Sullivan, M. 2010, *ApJ*, 709, 1067
Brinchmann, J., Charlot, S., White, S. D. M., et al. 2004, *MNRAS*, 351, 1151
Casteels, K. R. V., Conselice, C. J., Bamford, S. P., et al. 2014, *MNRAS*, 445, 1157
Cen, R., & Safarzadeh, M. 2015, *ApJL*, 798, L38
Cheng, T.-Y., Conselice, C. J., Aragón-Salamanca, A., et al. 2020, *MNRAS*, 493, 4209
Cheung, E., Trump, J. R., Athanassoula, E., et al. 2015, *MNRAS*, 447, 506
Chowdhury, R. K., Chatterjee, S., Lonappan, A. I., Khandai, N., & DiMatteo, T. 2020, *ApJ*, 889, 60
Churazov, E., Sazonov, S., Sunyaev, R., et al. 2005, *MNRAS*, 363, L91
Cigan, P. 2019, MultiColorFits: Colorize and Combine Multiple Fits Images for Visually Aesthetic Scientific Plots, Astrophysics Source Code Library, ascl:1909.002
Cisternas, M., Jahnke, K., Inskip, K. J., et al. 2011, *ApJ*, 726, 57
Cisternas, M., Sheth, K., Salvato, M., et al. 2015, *ApJ*, 802, 137
Condorcet, J.-A.-N. D. C., Sommerlad, F., & McLean, I. 1989, University of Oxford, Faculty of Social Studies. 1989, The political theory of Condorcet (Oxford: University of Oxford, Faculty of Social Studies)
Condorcet, J.-A.-N. d. C. . . m. d. A. d. t. 1785, Essai sur l'application de l'analyse à la probabilité des décisions rendues à la pluralité des voix ([Reprod.] / par M. le marquis de Condorcet, ... (Paris: de l'Imprimerie royale), <https://gallica.bnf.fr/ark:/12148/bpt6k417181>
Conroy, C., & White, M. 2013, *ApJ*, 762, 70
Cotini, S., Ripamonti, E., Caccianiga, A., et al. 2013, *MNRAS*, 431, 2661
Dashyan, G., Choi, E., Somerville, R. S., et al. 2019, *MNRAS*, 487, 5889
Davies, J. J., Crain, R. A., Oppenheimer, B. D., & Schaye, J. 2020, *MNRAS*, 491, 4462
Davis, B. L., Graham, A. W., & Cameron, E. 2018, *ApJ*, 869, 113
Davis, B. L., Graham, A. W., & Cameron, E. 2019, *ApJ*, 873, 85
de Nicola, S., Marconi, A., & Longo, G. 2019, *MNRAS*, 490, 600
Delvecchio, I., Lutz, D., Berta, S., et al. 2015, *MNRAS*, 449, 373
Di Matteo, T., Springel, V., & Hernquist, L. 2005, *Natur*, 433, 604
Ding, X., Silverman, J., Treu, T., et al. 2020, *ApJ*, 888, 37
Donley, J. L., Kartaltepe, J., Kocevski, D., et al. 2018, *ApJ*, 853, 63
Duncan, K., Conselice, C. J., Mundy, C., et al. 2019, *ApJ*, 876, 110
Ellison, S. L., Viswanathan, A., Patton, D. R., et al. 2019, *MNRAS*, 487, 2491
Emerson, P. 2013, *Social Choice and Welfare*, 40, 353
Erben, T., Schirmer, M., Dietrich, J. P., et al. 2005, *AN*, 326, 432
Fan, L., Han, Y., Fang, G., et al. 2016, *ApJL*, 822, L32
Fanidakis, N., Baugh, C. M., Benson, A. J., et al. 2012, *MNRAS*, 419, 2797
Furlong, M., Bower, R. G., Theuns, T., et al. 2015, *MNRAS*, 450, 4486
Gabor, J. M., Impey, C. D., Jahnke, K., et al. 2009, *ApJ*, 691, 705
Gao, F., Wang, L., Pearson, W. J., et al. 2020, *A&A*, 637, A94
Georgakakis, A., Coil, A. L., Laird, E. S., et al. 2009, *MNRAS*, 397, 623
Glikman, E., Simmons, B., Maily, M., et al. 2015, *ApJ*, 806, 218
Goulding, A. D., Greene, J. E., Bezanson, R., et al. 2018, *PASJ*, 70, S37
Goulding, A. D., Matthaey, E., Greene, J. E., et al. 2017, *ApJ*, 843, 135
Graham, A. W., & Scott, N. 2013, *ApJ*, 764, 151
Grogin, N. A., Conselice, C. J., Chazichristou, E., et al. 2005, *ApJL*, 627, L97
Grogin, N. A., Kocevski, D. D., Faber, S. M., et al. 2011, *ApJS*, 197, 35
Habouzit, M., Genel, S., Somerville, R. S., et al. 2019, *MNRAS*, 484, 4413
Häring, N., & Rix, H.-W. 2004, *ApJL*, 604, L89
Harrison, C. M., Costa, T., Tadhunter, C. N., et al. 2018, *NatAs*, 2, 198
Henriques, B. M. B., White, S. D. M., Thomas, P. A., et al. 2015, *MNRAS*, 451, 2663
Hewlett, T., Villforth, C., Wild, V., et al. 2017, *MNRAS*, 470, 755
Hirschmann, M., Dolag, K., Saro, A., et al. 2014, *MNRAS*, 442, 2304
Hong, J., Im, M., Kim, M., & Ho, L. C. 2015, *ApJ*, 804, 34
Hopkins, P. F., & Hernquist, L. 2009, *ApJ*, 698, 1550
Hopkins, P. F., Hernquist, L., Cox, T. J., et al. 2006a, *ApJS*, 163, 1
Hopkins, P. F., Hernquist, L., Cox, T. J., & Kereš, D. 2008, *ApJS*, 175, 356
Hopkins, P. F., Hernquist, L., Martini, P., et al. 2005, *ApJL*, 625, L71
Hopkins, P. F., & Quataert, E. 2010, *MNRAS*, 407, 1529
Hopkins, P. F., Richards, G. T., & Hernquist, L. 2007, *ApJ*, 654, 731
Hopkins, P. F., Somerville, R. S., Hernquist, L., et al. 2006b, *ApJ*, 652, 864
Hunter, J. D. 2007, *CSE*, 9, 90
Husemann, B., & Harrison, C. M. 2018, *NatAs*, 2, 196
Jahnke, K., Bongiorno, A., Brusa, M., et al. 2009, *ApJL*, 706, L215
Jahnke, K., & Macciò, A. V. 2011, *ApJ*, 734, 92
Johansson, P. H., Burkert, A., & Naab, T. 2009a, *ApJL*, 707, L184
Johansson, P. H., Naab, T., & Burkert, A. 2009b, *ApJ*, 690, 802
Joye, W. A., & Mandel, E. 2003, in ASP Conf. Ser. 295, Astronomical Data Analysis Software and Systems XII, ed. H. E. Payne, I. Jedrzejewski, & R. N. Hook (San Francisco, CA: ASP), 489
Jung, M., Illenseer, T. F., & Duschl, W. J. 2018, *A&A*, 614, A105
Karouzos, M., Jarvis, M. J., & Bonfield, D. 2014, *MNRAS*, 439, 861
Kauffmann, G., Heckman, T. M., White, S. D. M., et al. 2003, *MNRAS*, 341, 33
Kocevski, D. D., Faber, S. M., Mozena, M., et al. 2012, *ApJ*, 744, 148
Koekemoer, A. M., Faber, S. M., Ferguson, H. C., et al. 2011, *ApJS*, 197, 36
Kormendy, J., & Ho, L. C. 2013, *ARA&A*, 51, 511
Koss, M., Mushotzky, R., Veilleux, S., & Winter, L. 2010, *ApJL*, 716, L125
Koss, M. J., Blecha, L., Bernhard, P., et al. 2018, *Natur*, 563, 214
Lacey, C. G., Baugh, C. M., Frenk, C. S., et al. 2016, *MNRAS*, 462, 3854
Li, Y., Gendron-Marsolais, M.-L., Zhuravleva, I., et al. 2020b, *ApJL*, 889, L1
Li, Y., Habouzit, M., Genel, S., et al. 2020a, *ApJ*, 895, 102
López-Sanjuán, C., Balcells, M., Pérez-González, P. G., et al. 2009, *A&A*, 501, 505
Lotz, J. M., Davis, M., Faber, S. M., et al. 2008a, *ApJ*, 672, 177
Lotz, J. M., Jonsson, P., Cox, T. J., et al. 2011, *ApJ*, 742, 103
Lotz, J. M., Jonsson, P., Cox, T. J., & Primack, J. R. 2008b, *MNRAS*, 391, 1137
Madau, P., & Dickinson, M. 2014, *ARA&A*, 52, 415
Man, A. W. S., Zirm, A. W., & Toft, S. 2016, *ApJ*, 830, 89
Man, Z.-Y., Peng, Y.-J., Kong, X., et al. 2019, *MNRAS*, 488, 89
Marconi, A., & Hunt, L. K. 2003, *ApJL*, 589, L21

- Marian, V., Jahnke, K., Mechtley, M., et al. 2019, *ApJ*, 882, 141
- Martini, P. 2004, in *Coevolution of Black Holes and Galaxies*, ed. L. C. Ho (Cambridge: Cambridge Univ. Press), 169
- Martin-Navarro, I., Burchett, J. N., & Mezcuca, M. 2019, *ApJL*, 884, L45
- McAlpine, S., Bower, R. G., Rosario, D. J., et al. 2018, *MNRAS*, 481, 3118
- McAlpine, S., Harrison, C. M., Rosario, D. J., et al. 2020, *MNRAS*, 494, 5713
- McConnell, N. J., & Ma, C.-P. 2013, *ApJ*, 764, 184
- Mechtley, M., Jahnke, K., Windhorst, R. A., et al. 2016, *ApJ*, 830, 156
- Mundy, C. J., Conselice, C. J., Duncan, K. J., et al. 2017, *MNRAS*, 470, 3507
- Nelson, D., Pillepich, A., Springel, V., et al. 2019, *MNRAS*, 490, 3234
- Netzer, H. 2019, *MNRAS*, 488, 5185
- O'Leary, J. A., Moster, B. P., Naab, T., & Somerville, R. S. 2020, arXiv:2001.02687
- Oppenheimer, B. D., Davies, J. J., Crain, R. A., et al. 2020, *MNRAS*, 491, 2939
- Pillepich, A., Springel, V., Nelson, D., et al. 2018, *MNRAS*, 473, 4077
- Popping, G., Caputi, K. I., Trager, S. C., et al. 2015, *MNRAS*, 454, 2258
- Reilly, B. 2002, *International Political Science Review*, 23, 355
- Ricarte, A., Tremmel, M., Natarajan, P., & Quinn, T. 2019, *MNRAS*, 489, 802
- Rosario, D. J., McIntosh, D. H., van der Wel, A., et al. 2015, *A&A*, 573, A85
- Sabater, J., Best, P. N., & Argudo-Fernández, M. 2013, *MNRAS*, 430, 638
- Sahu, N., Graham, A. W., & Davis, B. L. 2019, *ApJ*, 887, 10
- Sanders, D. B., & Mirabel, I. F. 1996, *ARA&A*, 34, 749
- Sanders, D. B., Soifer, B. T., Elias, J. H., et al. 1988, *ApJ*, 325, 74
- Santini, P., Maiolino, R., Magnelli, B., et al. 2014, *A&A*, 562, A30
- Schawinski, K., Simmons, B. D., Urry, C. M., Treister, E., & Glikman, E. 2012, *MNRAS*, 425, L61
- Schawinski, K., Treister, E., Urry, C. M., et al. 2011, *ApJL*, 727, L31
- Schirmer, M. 2013, *ApJS*, 209, 21
- Schulze, A., Bongiorno, A., Gavignaud, I., et al. 2015, *MNRAS*, 447, 2085
- Schulze, A., Silverman, J. D., Daddi, E., et al. 2019, *MNRAS*, 488, 1180
- Schulze, A., & Wisotzki, L. 2010, *A&A*, 516, A87
- Schulze, M. 2011, *Social Choice and Welfare*, 36, 267
- Schulze, M. 2018, arXiv:1804.02973
- Shankar, F., Weinberg, D. H., Marsden, C., et al. 2020, *MNRAS*, 493, 1500
- Shen, Y., Richards, G. T., Strauss, M. A., et al. 2011, *ApJS*, 194, 45
- Shen, Y., Strauss, M. A., Oguri, M., et al. 2007, *AJ*, 133, 2222
- Sijacki, D., Vogelsberger, M., Genel, S., et al. 2015, *MNRAS*, 452, 575
- Silk, J., & Rees, M. J. 1998, *A&A*, 331, 1
- Silverman, J. D., Kampeczyk, P., Jahnke, K., et al. 2011, *ApJ*, 743, 2
- Smethurst, R. J., Simmons, B. D., Lintott, C. J., & Shanahan, J. 2019, *MNRAS*, 489, 4016
- Snyder, G. F., Rodriguez-Gomez, V., Lotz, J. M., et al. 2019, *MNRAS*, 486, 3702
- Somerville, R. S., Hopkins, P. F., Cox, T. J., Robertson, B. E., & Hernquist, L. 2008, *MNRAS*, 391, 481
- Springel, V., Di Matteo, T., & Hernquist, L. 2005, *MNRAS*, 361, 776
- Steinborn, L. K., Hirschmann, M., Dolag, K., et al. 2018, *MNRAS*, 481, 341
- Terrazas, B. A., Bell, E. F., Pillepich, A., et al. 2020, *MNRAS*, 493, 1888
- Treister, E., Schawinski, K., Urry, C. M., & Simmons, B. D. 2012, *ApJL*, 758, L39
- Truong, N., Pillepich, A., Werner, N., et al. 2020, *MNRAS*, 494, 549
- Urbano-Mayorga, J. J., Villar Martín, M., Buitrago, F., et al. 2019, *MNRAS*, 483, 1829
- Urrutia, T., Lacy, M., & Becker, R. H. 2008, *ApJ*, 674, 80
- Valentini, M., Murante, G., Borgani, S., et al. 2020, *MNRAS*, 491, 2779
- van der Wel, A., Franx, M., van Dokkum, P. G., et al. 2014, *ApJ*, 788, 28
- Ventou, E., Contini, T., Bouché, N., et al. 2017, *A&A*, 608, A9
- Ventou, E., Contini, T., Bouché, N., et al. 2019, *A&A*, 631, A87
- Vestergaard, M., & Peterson, B. M. 2006, *ApJ*, 641, 689
- Villforth, C., Hamann, F., Rosario, D. J., et al. 2014, *MNRAS*, 439, 3342
- Villforth, C., Hamilton, T., Pawlik, M. M., et al. 2017, *MNRAS*, 466, 812
- Villforth, C., Herbst, H., Hamann, F., et al. 2019, *MNRAS*, 483, 2441
- Weigel, A. K., Schawinski, K., Treister, E., Trakhtenbrot, B., & Sanders, D. B. 2018, *MNRAS*, 476, 2308
- Weinberger, R., Springel, V., Pakmor, R., et al. 2018, *MNRAS*, 479, 4056
- Wild, V., Heckman, T., & Charlot, S. 2010, *MNRAS*, 405, 933
- Xu, C. K., Zhao, Y., Scoville, N., et al. 2012, *ApJ*, 747, 85
- Yue, M., Fan, X., Schindler, J.-T., McGreer, I. D., & Huang, Y.-H. 2019, *ApJ*, 883, 141
- Zhao, D., Ho, L. C., Zhao, Y., Shanguan, J., & Kim, M. 2019, *ApJ*, 877, 52